

University of Dundee

## Highly Selective PTK2 Proteolysis Targeting Chimeras to Probe Focal Adhesion Kinase Scaffolding Functions

Popow, Johannes; Arnhof, Heribert; Bader, Gerd; Berger, Helmut; Ciulli, Alessio; Covini, David

*Published in:*  
Journal of Medicinal Chemistry

*DOI:*  
[10.1021/acs.jmedchem.8b01826](https://doi.org/10.1021/acs.jmedchem.8b01826)

*Publication date:*  
2019

*Document Version*  
Peer reviewed version

[Link to publication in Discovery Research Portal](#)

### *Citation for published version (APA):*

Popow, J., Arnhof, H., Bader, G., Berger, H., Ciulli, A., Covini, D., Dank, C., Gmaschitz, T., Greb, P., Karolyi-Özguer, J., Koegl, M., McConnell, D. B., Pearson, M., Rieger, M., Rinnenthal, J., Roessler, V., Schrenk, A., Spina, M., Steurer, S., ... Ettmayer, P. (2019). Highly Selective PTK2 Proteolysis Targeting Chimeras to Probe Focal Adhesion Kinase Scaffolding Functions. *Journal of Medicinal Chemistry*, 62(5), 2508–2520. <https://doi.org/10.1021/acs.jmedchem.8b01826>

### **General rights**

Copyright and moral rights for the publications made accessible in Discovery Research Portal are retained by the authors and/or other copyright owners and it is a condition of accessing publications that users recognise and abide by the legal requirements associated with these rights.

- Users may download and print one copy of any publication from Discovery Research Portal for the purpose of private study or research.
- You may not further distribute the material or use it for any profit-making activity or commercial gain.
- You may freely distribute the URL identifying the publication in the public portal.

### **Take down policy**

If you believe that this document breaches copyright please contact us providing details, and we will remove access to the work immediately and investigate your claim.

## Highly Selective PTK2 Proteolysis Targeting Chimeras (PROTACs) to Probe Focal Adhesion Kinase Scaffolding Functions

Johannes Popow, Heribert Arnhof, Gerd Bader, Helmut Berger, Alessio Ciulli, David Covini, Christian Dank, Teresa Gmaschitz, Peter Greb, Jale Karolyi-Oezguer, Manfred Koegl, Darryl McConnell, Mark Pearson, Maria Rieger, Jörg Rinnenthal, Vanessa Roessler, Andreas Schrenk, Markus Spina, Steffen Steurer, Nicole Trainor, Elisabeth Traxler, Corinna Wieshofer, Andreas Zoephel, and Peter Ettmayer

*J. Med. Chem.*, **Just Accepted Manuscript** • DOI: 10.1021/acs.jmedchem.8b01826 • Publication Date (Web): 09 Feb 2019

Downloaded from <http://pubs.acs.org> on February 10, 2019

### Just Accepted

“Just Accepted” manuscripts have been peer-reviewed and accepted for publication. They are posted online prior to technical editing, formatting for publication and author proofing. The American Chemical Society provides “Just Accepted” as a service to the research community to expedite the dissemination of scientific material as soon as possible after acceptance. “Just Accepted” manuscripts appear in full in PDF format accompanied by an HTML abstract. “Just Accepted” manuscripts have been fully peer reviewed, but should not be considered the official version of record. They are citable by the Digital Object Identifier (DOI®). “Just Accepted” is an optional service offered to authors. Therefore, the “Just Accepted” Web site may not include all articles that will be published in the journal. After a manuscript is technically edited and formatted, it will be removed from the “Just Accepted” Web site and published as an ASAP article. Note that technical editing may introduce minor changes to the manuscript text and/or graphics which could affect content, and all legal disclaimers and ethical guidelines that apply to the journal pertain. ACS cannot be held responsible for errors or consequences arising from the use of information contained in these “Just Accepted” manuscripts.

1  
2  
3  
4  
5  
6  
7  
8  
9  
10  
11  
12  
13  
14  
15  
16  
17  
18  
19  
20  
21  
22  
23  
24  
25  
26  
27  
28  
29  
30  
31  
32

# Highly Selective PTK2 Proteolysis Targeting Chimeras (PROTACs) to Probe Focal Adhesion Kinase Scaffolding Functions.

33  
34  
35  
36  
37  
38  
39  
40  
41  
42  
43  
44  
45  
46  
47  
48  
49

*Johannes Popow<sup>1</sup>, Heribert Arnhof<sup>1</sup>, Gerd Bader<sup>1</sup>, Helmut Berger<sup>1</sup>, Alessio Ciulli<sup>2</sup>, David Covini<sup>1</sup>, Christian Dank<sup>1</sup>, Teresa Gmaschitz<sup>1</sup>, Peter Greb<sup>1</sup>, Jale Karolyi-Özguer<sup>1</sup>, Manfred Koegl<sup>1</sup>, Darryl B. McConnell<sup>1</sup>, Mark Pearson<sup>1</sup>, Maria Rieger, Joerg Rinnenthal<sup>1</sup>, Vanessa Roessler<sup>1</sup>, Andreas Schrenk<sup>1</sup>, Markus Spina<sup>1</sup>, Steffen Steurer<sup>1</sup>, Nicole Trainor<sup>2</sup>, Elisabeth Traxler<sup>1</sup>, Corinna Wieshofer<sup>1</sup>, Andreas Zoephel<sup>1</sup>, Peter Ettmayer<sup>1\*</sup>*

50  
51  
52  
53  
54  
55  
56  
57  
58  
59  
60

<sup>1</sup>Boehringer Ingelheim RCV GmbH & Co KG, 1221 Vienna, Austria

<sup>2</sup>Division of Biological Chemistry and Drug Discovery, School of Life Sciences, James Black Centre, University of Dundee, Dow Street, DD1 5EH, Dundee, Scotland, United Kingdom

\*corresponding author, E-mail: peter.ettmayer@boehringer-ingelheim.com

## KEYWORDS

PROTACs, protein degradation, E3 ubiquitin ligases, kinases, von Hippel-Lindau, Cereblon, CRBN

1  
2  
3  
4  
5  
6  
7  
8  
9  
10  
11  
12  
13  
14  
15  
16  
17  
18  
19  
20  
21  
22  
23  
24  
25  
26  
27  
28  
29  
30  
31  
32  
33  
34  
35  
36  
37  
38  
39  
40  
41  
42  
43  
44  
45  
46  
47  
48  
49  
50  
51  
52  
53  
54  
55  
56  
57  
58  
59  
60

**ABSTRACT**

The focal adhesion tyrosine kinase (PTK2) is often over-expressed in human hepatocellular carcinoma (HCC) and several reports have linked PTK2 depletion and/or pharmacological inhibition to reduced tumorigenicity. However, the clinical relevance of targeting PTK2 still remains to be proven. Here we present two highly selective and functional PTK2 PROTACs utilizing VHL and cereblon ligands to hijack E3 ligases for PTK2 degradation. BI-3663 (cereblon-based) degrades PTK2 with a median  $DC_{50}$  of 30 nM to > 80 % across a panel of eleven HCC cell lines. Despite effective PTK2 degradation, these compounds did not phenocopy the reported anti-proliferative effects of PTK2 depletion in any of the cell lines tested. By disclosing these compounds, we hope to provide valuable tools for the study of PTK2 degradation across different biological systems.

## Introduction

Focal adhesion tyrosine kinase (PTK2) is a cytoplasmic protein tyrosine kinase that is overexpressed and activated in many types of advanced-stage solid cancers. PTK2 is reported to play an important role in adhesion, spreading, motility, invasion, metastasis, survival, angiogenesis, epithelial to mesenchymal transition (EMT), cancer stem cells and the tumour microenvironment<sup>1,2</sup>. Overexpression and activation of PTK2 is associated with several human malignant diseases, including colorectal<sup>3</sup>, ovarian<sup>4</sup>, esophageal<sup>5</sup> and hepatocellular carcinoma (HCC)<sup>6</sup> and is correlated with poor overall patient survival<sup>7, 8</sup>. Hepatocellular carcinoma (HCC) is the most common type of liver cancer in humans, accounting for 70–85 % of primary liver malignancies, and is the third leading cause of cancer-related death worldwide<sup>9, 10</sup>. HCC is associated with an extremely poor prognosis since it is often diagnosed at advanced stages, restricting the currently available therapeutic options to either surgical resection or liver transplantation<sup>11, 12</sup>. Several reports link PTK2 depletion or pharmacological inhibition of its kinase activity to reduction of *in vitro* and *in vivo* tumorigenicity in HCC models<sup>13, 14</sup>. However, the disconnect between modulation of intracellular PTK2 autophosphorylation and growth inhibition as well as the often suboptimal selectivity profile of the inhibitors used makes it difficult to link the reported blockade of HCC tumour initiation and maintenance to PTK2 inhibition.

We previously described BI-853520, a novel ATP-competitive inhibitor distinguished by high potency and selectivity<sup>15, 16</sup>. BI-853520 inhibits PTK2 autophosphorylation in cancer cell lines and blocks anchorage-independent proliferation with single digit nmol/L potency. In contrast, cells grown in conventional surface (2-D) culture were found to be 1,000-fold less sensitive to BI-853520. These findings are in keeping with the described role of PTK2 in integrin mediated

1  
2  
3 signaling<sup>2, 17</sup>. We reasoned that ligands derived from BI-853520 would be suitable to develop  
4  
5 PROTACs (PROteolysis TArgeting Chimeras) and compare the potential anti-oncogenic effects  
6  
7 of PTK2 depletion as compared to inhibition of its kinase activity<sup>18</sup>.  
8  
9

10 PROTACs are bifunctional degrader molecules composed of a ligand for the target protein  
11  
12 linked to a module that recruits an E3 ligase<sup>19, 20</sup>. PROTACs represent an emerging therapeutic  
13  
14 strategy to use small molecules to deplete a protein by repurposing the ubiquitin-proteasome  
15  
16 system<sup>21, 22</sup>. Upon formation of a ternary complex target:PROTAC:E3 ligase<sup>23-25</sup>, the protein of  
17  
18 interest is ubiquitinated and subsequently degraded by the proteasome. Compared to  
19  
20 pharmacological inhibition of the kinase function, protein degradation more closely resembles  
21  
22 genetic approaches to interfere with PTK2 expression in HCC models. Moreover, PROTAC  
23  
24 molecules can add a layer of target selectivity beyond that expected from the constitutive binding  
25  
26 ligands, thus providing highly selective degraders with potentially reduced off-target effects<sup>25-28</sup>.  
27  
28  
29

30 The most common E3 ligases currently recruited using PROTACs are the von Hippel-Lindau  
31  
32 (VHL) protein complex CRL2<sup>VHL</sup> and the cereblon (CRBN) complex CRL4<sup>CRBN</sup>. PROTACs  
33  
34 consisting of the same target ligand but employing either VHL or CRBN ligands can exhibit  
35  
36 different degradation selectivity and efficacy<sup>26, 29-31</sup>. Emerging evidence suggests that it might be  
37  
38 beneficial to develop parallel chemical series hijacking different E3 ligases. First, expression of  
39  
40 the recruited E3 ligase and intrinsic activity may be context-dependent and vary widely amongst  
41  
42 cell- and tissue types<sup>32</sup>. Second, resistance mechanisms could potentially arise from loss of the  
43  
44 recruited E3 ligase, as demonstrated by the correlation between level of CRBN and response to  
45  
46 CRBN-recruiting drugs in multiple myeloma<sup>33</sup>. Flexible choice of the recruited E3 ligase may  
47  
48 therefore aid targeted protein degradation.  
49  
50  
51  
52  
53  
54  
55  
56  
57  
58  
59  
60

1  
2  
3 Recently, the first PTK2 PROTACs have been reported. Conjugating the known pyrimidine-  
4 based ALK inhibitors, TAE684 and LDK378, to the cereblon ligand pomalidomide led to the  
5 discovery of the first small molecule degraders of ALK that concomitantly degrade, PTK2,  
6 Aurora A, FER, and RPS6KA1<sup>34</sup>. A PROTAC based on a highly promiscuous kinase inhibitor  
7 was also reported to degrade PTK2 amongst 27 additional kinases<sup>35</sup>. While both studies  
8 demonstrate that PTK2 can be targeted by a PROTAC approach, they also clearly highlight the  
9 need for more selective PTK2 PROTACs to address its role in cancer. Motivated by the potential  
10 of targeting kinase-independent functions of PTK2 with a low molecular weight modality, we  
11 initiated a PROTAC medicinal chemistry campaign to artificially recruit PTK2 to two different  
12 E3 ligases.  
13  
14  
15  
16  
17  
18  
19  
20  
21  
22  
23  
24  
25

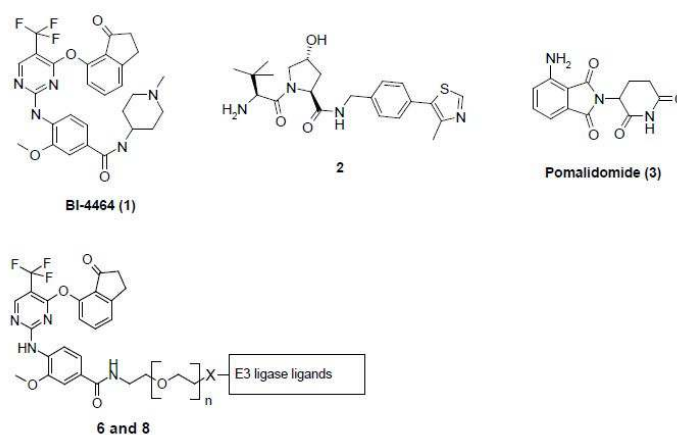
26 Here, we show the synthesis and characterization of the first probe-quality PROTACs targeting  
27 PTK2. Structure-guided conjugation of a highly selective PTK2 inhibitor to either a CRBN or  
28 VHL ligand led to selective PTK2 degraders. We profiled both PROTACs for degradation  
29 efficacy and anti-proliferative activity in a panel of HCC, tongue squamous cell carcinoma,  
30 melanoma, pancreatic ductal adenocarcinoma and non-small cell lung cancer cell lines several of  
31 which were recently shown to depend on expression of PTK2 by functional RNA interference  
32 screening<sup>36</sup>. Despite potent and complete degradation of PTK2, both degraders failed to show the  
33 anticipated growth reduction beyond the effect of a PTK2 kinase inhibitor in these models.  
34  
35  
36  
37  
38  
39  
40  
41  
42  
43  
44

## 45 **Results and Discussion**

46 We designed a set of PTK2 PROTACs recruiting the two E3 ubiquitin ligases, VHL and  
47 CRBN, to test whether PTK2 can be targeted by targeted proteolysis. Making use of available E3  
48 ligase ligands, we aimed at maximizing the chance of developing an active PTK2 degrader tool  
49 compound. We selected the highly selective ATP competitive inhibitor BI-4464 (**1**, Scheme 1), a  
50  
51  
52  
53  
54  
55  
56  
57  
58  
59  
60



1  
2  
3 close analogue of the 2-aminophenyl-4-phenoxy pyrimidine BI-853520<sup>15</sup> currently being tested in  
4  
5 clinical trials as a PTK2 ligand. The choice of BI-4464 as a target ligand was driven by its high  
6  
7 binding affinity and exquisite selectivity across a large kinase panel (see also Figure 3). We  
8  
9 believe that this exceptional selectivity originates from a unique binding mode which seems to be  
10  
11 less tolerated by other kinases. To design a first generation of degraders, we inspected the crystal  
12  
13 structure of BI-4464 bound to the PTK2 kinase domain to identify suitable attachment points and  
14  
15 vectors for linker conjugation (Figure 1). The structure shows binding of the trifluoro-  
16  
17 aminopyrimidine moiety to the backbone nitrogen and carbonyl of cysteine 502 in the hinge  
18  
19 region via two hydrogen bonds. In addition, the oxygen of the dihydroindenone moiety forms  
20  
21 another hydrogen bond to the backbone nitrogen of aspartic acid 564. The N-methyl piperidine  
22  
23 group of BI-4464 was identified as solvent-exposed and not involved in any interactions with the  
24  
25 protein. We further selected **2**<sup>37</sup> and pomalidomide **3**,<sup>38</sup> (Scheme 1) as VHL and CRBN ligands,  
26  
27 respectively. Their terminal amino groups (Table 1 and Scheme 1) were conjugated *via* an amide  
28  
29 bond to the linker consisting of up to five PEG units without perturbing the interaction with the  
30  
31 E3 ligases, as previously demonstrated<sup>28, 31, 39, 40</sup>.  
32  
33  
34  
35  
36  
37  
38  
39  
40  
41  
42  
43  
44  
45  
46  
47  
48  
49  
50  
51  
52  
53  
54



55  
56  
57  
58  
59  
60

**Scheme 1.** Chemical structures of BI-4464 ligand **1**, VHL ligand **2**<sup>37, 41, 42</sup> and CRBN ligand **3**<sup>38</sup>.

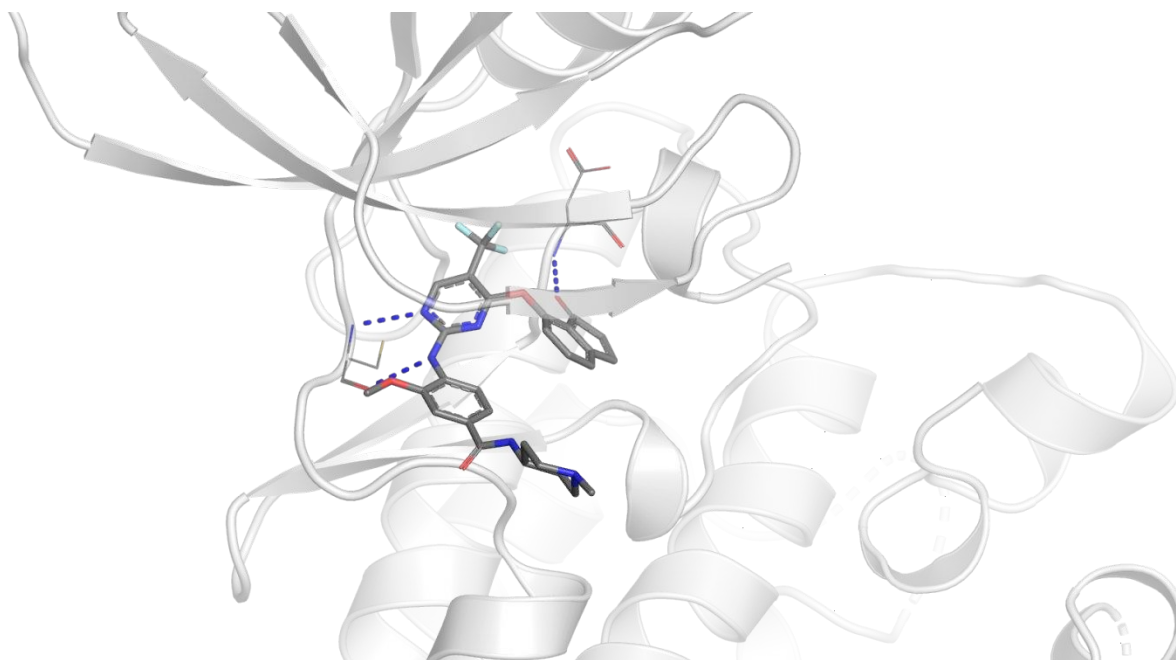


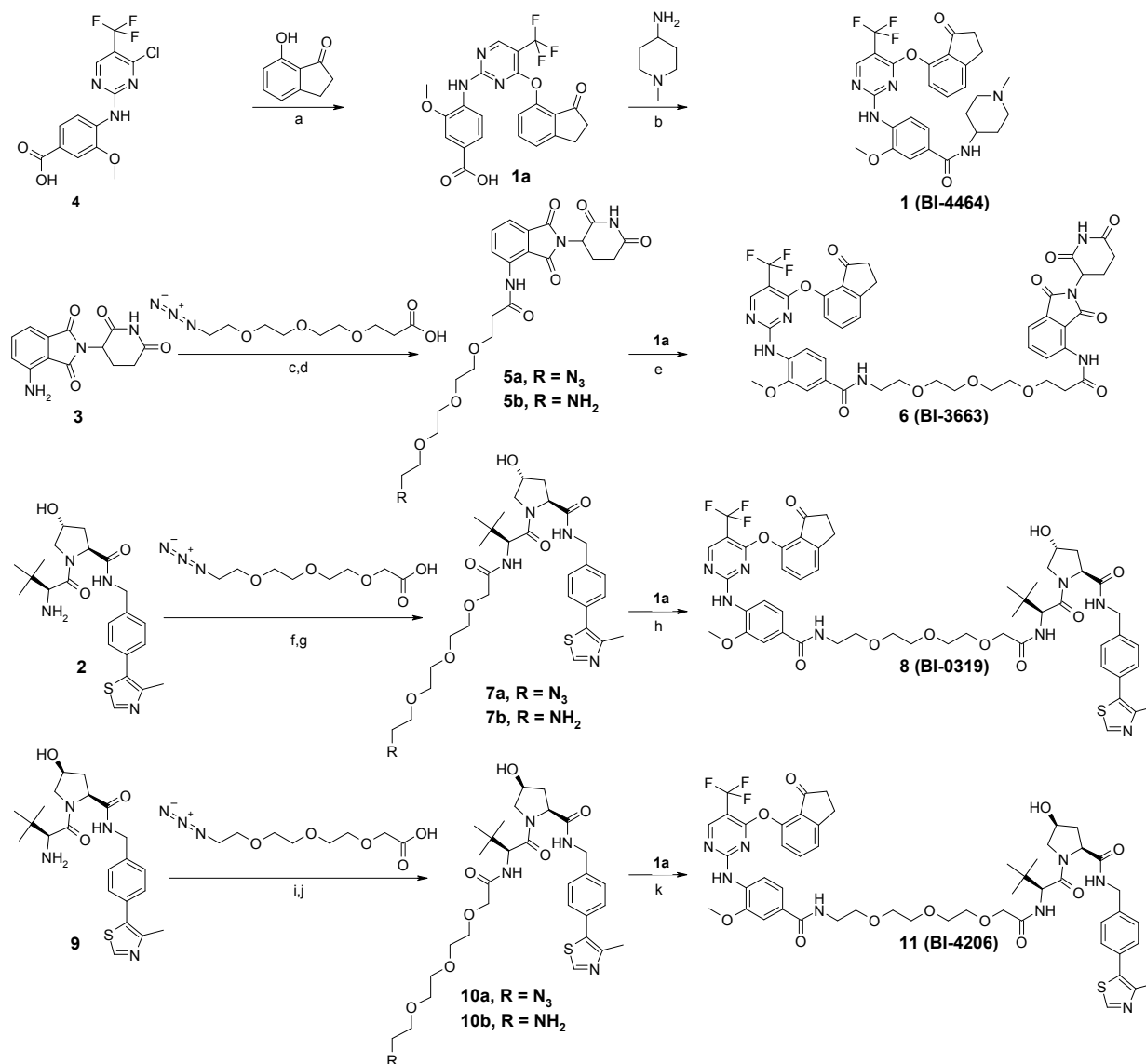
**Figure 1.** Structure of BI-4464 bound to PTK2 (PDB ID 6I8Z). Hydrogen bonds to cysteine 502 and aspartic acid 564 are depicted in blue.

To obtain the described compounds **6** and **8** (Table 1), a convergent synthesis was developed to connect **1a** to each E3 ligase ligand **2** and **3**. PEG linkers 1-5 (Scheme 2 shows an example of linker length three) were synthesized and profiled. The synthesis of ligand **1a** was carried out as outlined in Scheme 2. Aromatic nucleophilic substitution of the 4-chloropyrimidine **4** with 7-hydroxy-2,3-dihydroindan-1-one produced the carboxylic acid **1a**. Amide coupling of azido-PEG-3-propanoic acid and azido-PEG-3-acetic acid to the E3 ligase ligand **2** and **3** followed by catalytic hydrogenation produced the amines **5b**, **7b** and **10b** in good yields. The final PROTACs **6**, **8** and the cis-VHL analogue **11** were synthesized following amide coupling of the ligase linker conjugates **5b**, **7b** and **10b** with **1a**.

**Table 1.** Binary affinities of compounds **1**, **6**, **8** for PTK2 and the respective PTK2 degradation data in A549 cells.

Code	N	X	E3 ligase ligand	PTK2* pIC <sub>50</sub>	A549 cells, 18h**	
					pDC <sub>50</sub>	D <sub>max</sub> [%]
<b>1 (BI-4464)</b>	-	-	-	7.8 ± 0.1	>10,000	-
<b>6 (BI-3663)</b>	3	CONH	POMA	7.7 ± 0.1	7.6 ± 0.1	95 ± 4
<b>8 (BI-0319)</b>	2	O-CH <sub>2</sub> - CONH	2	7.7 ± 0.1	6.7 ± 0.4	80 ± 9

\* Thermo Fisher selectScreen Kinase Profiling Services, Z'-Light, ATP@Km, pIC<sub>50</sub> ± STDEV \*\* Degradation activity is reported as concentration needed to achieve 50 % PTK2 protein degradation (pDC<sub>50</sub> ± STDEV) and maximal achievable protein degradation (D<sub>max</sub>) relative to DMSO. PTK2 levels were determined by protein capillary electrophoresis and normalized to GAPDH. (N = 3)

**Scheme 2.** Synthesis of the PTK2 degraders.<sup>a</sup>

<sup>a</sup>Reaction Conditions: (a) Cs<sub>2</sub>CO<sub>3</sub>, MgSO<sub>4</sub>, dioxane, 80°C, 16 h, 78%; (b) HATU, DIPEA, DMF, rt, 2 h, 75%; (c) T3P, pyridine, DMF, 80°C, 3h, 76%; (d) H<sub>2</sub> (6 bar), Pd/C (10%), MeOH, rt, 3 h, 90%; (e) **1a**, HATU, DIPEA, DMF, rt, 18 h, 10%; (f) HATU, DIPEA, DMF, rt, 1 h, 63%; (g) H<sub>2</sub> (5 bar), Pd/C (10%), MeOH, rt, 2.5 h, 82%; (h) **1a**, HATU, DIPEA, DMF, rt, 24 h, 34%; (i) HATU, DIPEA, DMF, rt, 2 h, 47%; (j) H<sub>2</sub> (6 bar), Pd/C (10%), MeOH, rt, 3 h, 98%; (k) **1a**, HATU, DIPEA, DMF, rt, 16 h, 69%.

1  
2  
3 We next tested PTK2 degradation by all synthesized PROTACs (sampling linker lengths of up  
4 to five ethylene glycol units) after 16 hours treatment of the human lung adenocarcinoma cell  
5 line A549. PROTACs **6** (BI-3663) and **8** (BI-0319) were identified as the best degraders in the  
6 CRBN and VHL series and characterized in greater detail. The CRBN-based PROTAC **6** (BI-  
7 3663) degraded PTK2 potently ( $DC_{50} = 27$  nM) with a maximally obtainable degradation at the  
8 chosen experimental conditions of 95% ( $D_{max}$ ) while the best VHL-based PROTAC **8** (BI-0319)  
9 only achieved partial degradation ( $D_{max} = 80$  %) and was less potent ( $DC_{50} = 243$  nM) in A549  
10 cells (Table 1 and Figure 2). Further, both PROTACs show a small apparent hook effect in A549  
11 cells at 25  $\mu$ M. Consistent with VHL dependency, which requires the substituents of the  
12 pyrrolidine in the VHL ligand in a *trans* configuration<sup>28</sup>, degradation of PTK2 by **8** (BI-0319)  
13 was abolished by switching the stereochemistry of the pyrrolidine substituents to the *cis*  
14 configuration (**11**, **BI-4206**) (Figure 2A). Moreover, as predicted for neddylation-dependent E3  
15 ligases such as VHL and CRBN, the NEDD8 inhibitor MLN4924<sup>43</sup> (MLN) inhibited degradation  
16 of PTK2 by **6** (BI-3663) and **8** (BI-0319) (Figure 2A and B). Importantly, the PTK2 ligand **1**  
17 itself did not affect PTK2 levels.

18  
19  
20  
21  
22  
23  
24  
25  
26  
27  
28  
29  
30  
31  
32  
33  
34  
35  
36  
37  
38 We assessed PTK2 target engagement *in vitro* to understand the effect of the linker and exit  
39 vector on PTK2 inhibition of PROTACs **6** and **8**. As predicted from the structure-based design,  
40 both PROTACs and the PTK2 ligand inhibited PTK2 *in vitro* with virtually identical potencies  
41 ( $IC_{50} = 18$  and 19 versus 17 nM for the PTK2 inhibitor **1**).

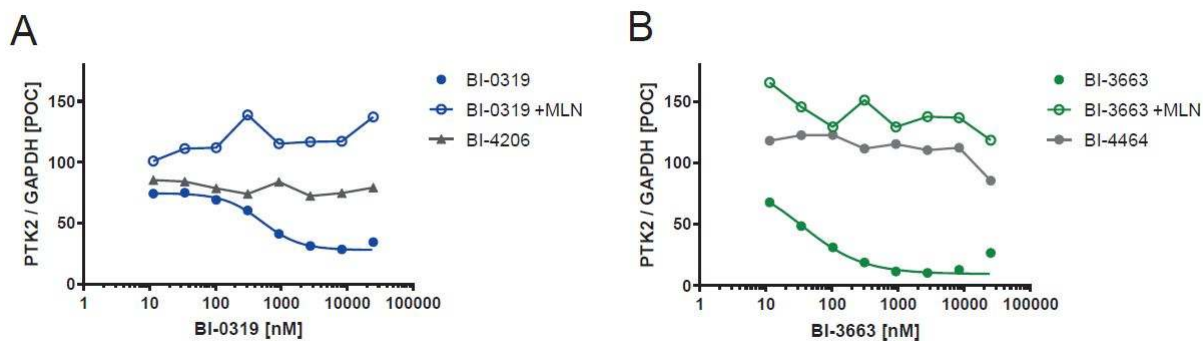


**Figure 2.** Characterization of BI-0319 and BI-3663 in A549 cells. A) A549 cells were treated with the indicated concentrations of BI-0319 in presence or absence of the NEDD8 inhibitor MLN4924 (MLN, 3  $\mu$ M) or an inactive stereoisomer (BI-4206) for 18 h. PTK2 levels were determined by protein capillary electrophoresis and normalized to GAPDH. Values are stated as percentages of DMSO controls (POC). B) A549 cells were treated with the indicated concentrations of BI-3663 in presence or absence of the NEDD8 inhibitor MLN4924 (3  $\mu$ M) or with the PTK2 inhibitor BI-4664 for 18 h. PTK2 levels were measured and are stated as in A.

In contrast to the previously published less selective PTK2 degraders<sup>34, 35</sup>, we believe that a defining aspect of the PTK2 degraders described here is their high selectivity, which should enable validation of the relevance of PTK2 scaffolding functions in biologically relevant contexts. Indeed, of the 397 kinases tested in a kinase panel screening only 2 were inhibited by more than 90 % at 1  $\mu$ M (Figure 3). Interestingly, BI-0319 (**8**) is more selective than the already highly selective PTK2 TKI **1** (BI-4464). We assume that the kinase selectivity panel for BI-3663 (**6**) might be comparable to BI-0319 since both exit vector and linker are identical for a distance of nine atoms from the piperidine moiety of the PTK2 ligand

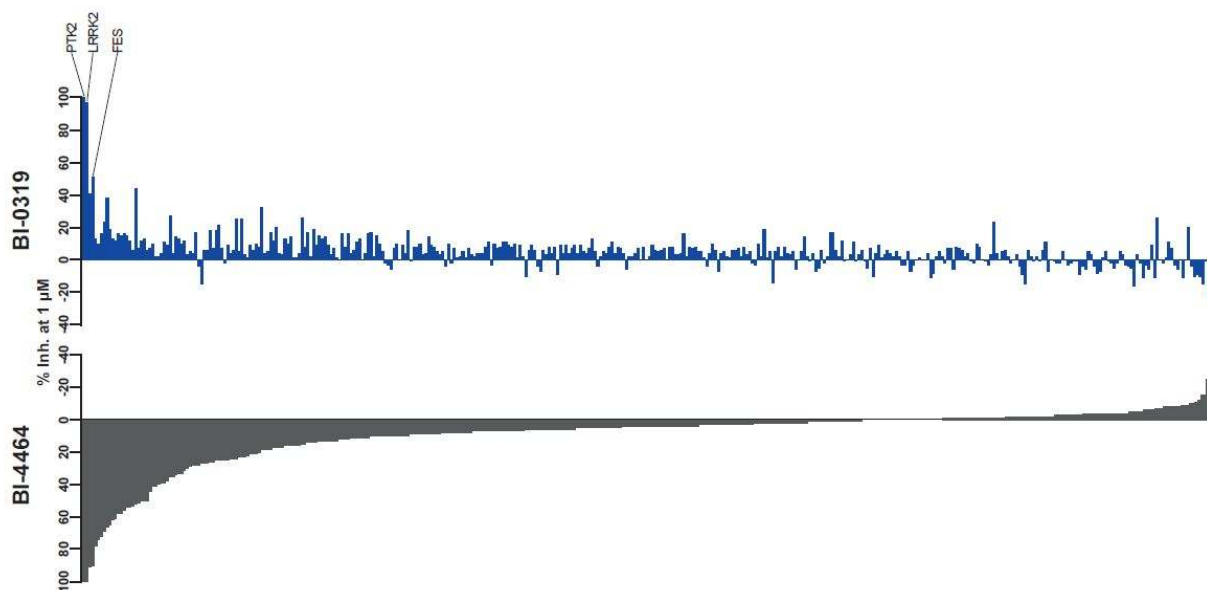


**Figure 3.** Kinase selectivity panels of the PTK2 ligand BI-4464 and VHL PROTAC BI-0319.

Bars indicate percent inhibition at 1  $\mu$ M of either compound.

We employed multiplexed isobaric tagging mass spectrometry to assess the cellular selectivity of BI-3663 (**6**) and BI-0319 (**8**) for PTK2 degradation and identify potential degradation off-targets in a quantitative and unbiased manner. Amongst the 6,008 proteins quantified in this analysis in A549 cells, PTK2 showed a distinct and significant change in abundance upon treatment with either PROTAC. (Figure 4 and Supplemental table 3). Neither BI-3663 (**6**) nor BI-0319 (**8**) induced any significant changes in abundance of other detectable kinases, thus confirming the high selectivity of both degraders within the kinase family. Of note, the two most prominent kinase off-targets of the inhibitor were not detected in this dataset. Interestingly BI-0319 (**8**) – but not BI-3663 (**6**) – also induced a significant change of PDE6D levels (Figure 4A), a finding corroborated by immunoblot in A549 cells (Supplemental figure 1).

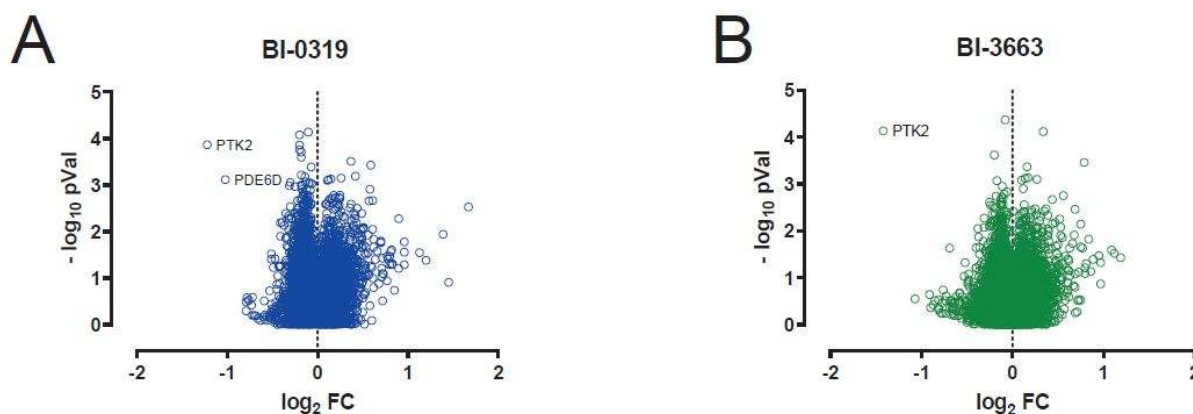


**Figure 4.** Total proteome analysis of A549 cells treated with 3  $\mu$ M of BI-0319 (A) or BI-3663 (B) for 18 h and compared to DMSO controls. Samples were run in biological triplicates and analyzed by mass spectrometry. Volcano plot displays  $\log_2$  of fold-change in abundance versus  $-\log_{10}$  of adjusted p value ( $N = 3$ ).

Having established the high selectivity of both PROTACs, in particular of the CRBN-based BI-3663, we tested their potential to degrade PTK2 in a panel of eleven HCC cell lines (Table 3 and Supplemental figure 2 and 3). Both PROTACs show comparable degradation potencies and efficacies in the 11 HCC cell lines tested (BI-3663 mean  $pDC_{50} = 7.45 \pm 0.60$  versus BI-0319 mean  $pDC_{50} = 7.08 \pm 0.52$ ). Whereas PTK2 levels in cell lines such as SNU-398 were equally sensitive to treatment with both PROTACs, other cell lines, such as Hep3B2.1-7 exhibited a  $>10$  fold difference of the potencies of **6** and **8** in cell-based PTK2 degradation assays, as observed for A549 cells during the profiling experiments (Figure 5 and Table 2).

It is not unexpected that heterobifunctional molecules unavoidably result in high molecular weight compounds, making it difficult to balance their physicochemical properties in a manner



1  
2  
3 consistent with acceptable permeability and solubility. While both PROTACs have a comparable  
4  
5 low aqueous solubility and high tPSA (241,243 Å<sup>2</sup>), PROTAC **6** has one hydrogen bond donor  
6  
7 (HBD) more than PROTAC **8**. The negative impact on permeability for **6** might be  
8  
9 compensated by the higher lipophilicity (ClogP 6.9 vs 3.8) however, the higher lipophilicity of **6**  
10  
11 also translates in higher PPB and lower free fraction (**6**: 4.0%, **8**: 11.3; Supplemental table 1).  
12  
13  
14  
15  
16

17 As assessed by the Caco2 assay, both PROTACs exhibit low permeability and significant  
18  
19 efflux (Supplemental table 1). Therefore, high efflux might compromise cellular exposures  
20  
21 achieved by both PROTACs. We reasoned that blocking multidrug efflux pumps (such as the  
22  
23 Multidrug-Resistance-Protein 1, PGP) might boost the potency and efficacy of both PROTACs  
24  
25 in cell lines with a large discrepancy between biochemical and intracellular activity.  
26  
27 Cyclosporine A (CsnA) has been described as a substrate of several drug transporters including  
28  
29 PGP<sup>44</sup> and can therefore be used to saturate these transporters at high concentrations.  
30  
31 Consequently, we assessed PTK2 degradation by both PROTACs upon addition of CsnA to  
32  
33 saturate drug transport in Hep3B2.1-7 (Figure 6A and B). Indeed, we observed a comparable  
34  
35 shift in the potency of PTK2 degradation for both PROTACs (Table 2), consistent with efflux  
36  
37 contributing to their reduced degradation efficacy in this cell line. Of note, CsnA only had a  
38  
39 minor effect on PTK2 levels (Figure 6C).  
40  
41  
42  
43  
44  
45  
46  
47  
48  
49  
50  
51  
52  
53  
54  
55  
56  
57  
58  
59  
60

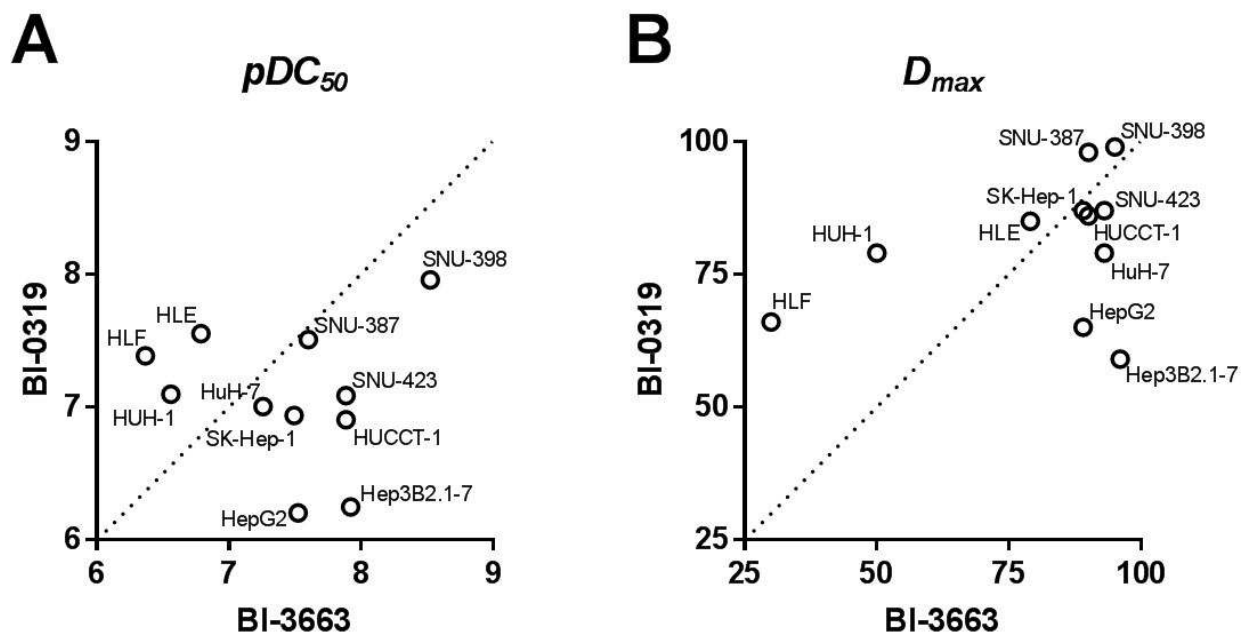


**Figure 5.** Cumulative analysis of half-maximal effective concentrations ( $DC_{50}$ , A) and maximal degree of PTK2 degradation ( $D_{max}$ , B) achieved by BI-0319 or BI-3663.  $pDC_{50}$  and  $D_{max}$  at 18 h were determined as indicated in supplemental figures 2 and 3.

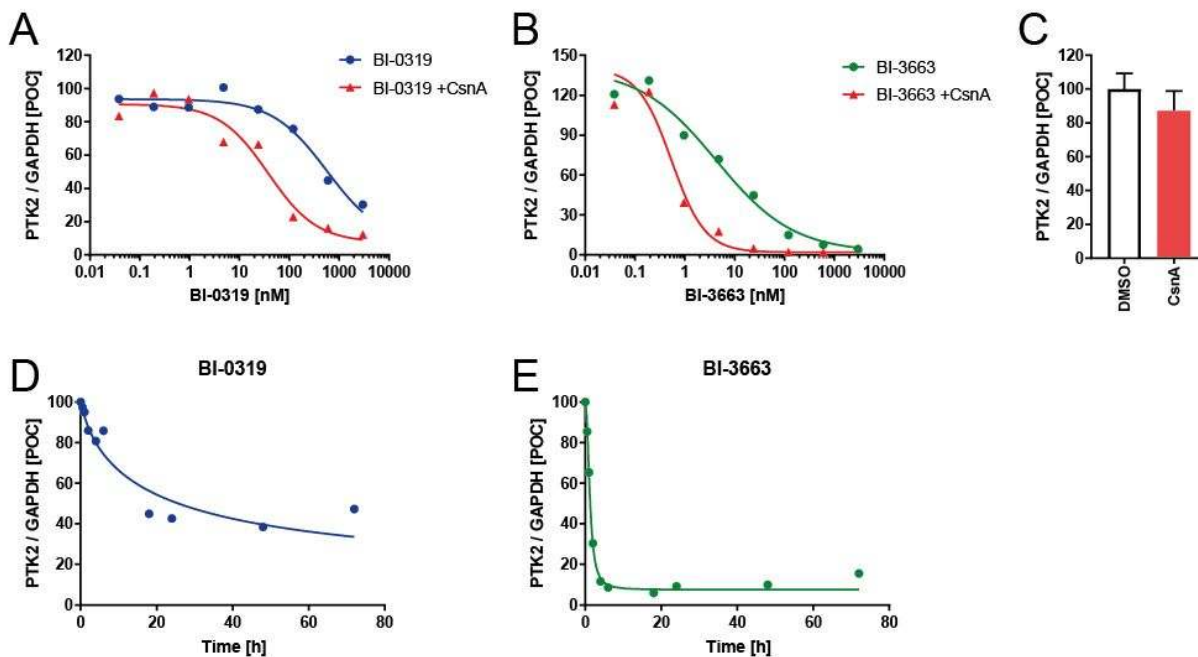


**Figure 6.** Analysis of PTK2 degradation in Hep3B2.1-7 cells. A) cells were treated with the indicated concentrations of BI-0319 for 18 h in presence (red triangles) or absence (blue circles) of 10  $\mu$ M cyclosporine A (CsnA). B) cells were treated for 18 h with the indicated concentrations of BI-3663 in presence (red triangles) or absence (green circles) of 10  $\mu$ M CsnA. C) cells were treated with 10  $\mu$ M CsnA for 18 h. D) Time course analysis of PTK2 levels in cells treated with 3  $\mu$ M BI-0319. E) Time course analysis of PTK2 levels in cells treated with 3  $\mu$ M BI-3663. Values state PTK2 protein levels normalized to GAPDH relative to DMSO (or CsnA only) controls.

**Table 2.** PTK2 degradation data of BI-3663 and BI-0319 in A549 and Hep3B2.1-7 cells.

	A549, 18 h*		Hep3B2.1-7, 18 h *		Hep3B2.1-7, 18 h * + 10 $\mu$ M CsnA	
	pDC <sub>50</sub>	D <sub>max</sub> [%]	pDC <sub>50</sub>	D <sub>max</sub> [%]	pDC <sub>50</sub>	D <sub>max</sub> [%]
<b>6 (BI- 3663)</b>	7.6 $\pm$ 0.1	95 $\pm$ 4	7.9	96	9.0	94
<b>8 (BI -0319)</b>	6.7 $\pm$ 0.4	80 $\pm$ 9	6.2	59	7.4	88

\* Degradation activity is reported as concentration needed to achieve 50 % PTK2 protein degradation (pDC<sub>50</sub>  $\pm$  STDEV) and maximal achievable protein degradation (D<sub>max</sub>) relative to DMSO.

PROTACs **6** and **8** differ considerably with respect to their cellular degradation rate in Hep3B2.1-7 cells. The CRBN-based PROTAC **6** achieved complete degradation of PTK2 after five hours whereas the VHL-based PROTAC **8** achieved maximal degradation only after 20 hours (Figure 6D and E). Of note, the CRBN-based PROTAC **6** was considerably less stable in cell assay buffer containing 10% FCS (M+18 and +32 observed) than the VHL-based PROTAC **8** (Supplemental Table 1). PROTAC **6** was found to be stable as a solid and in DMSO stock solution (>3 month, data not shown). Despite this previously reported instability of CRBN based PROTACs<sup>45</sup> PROTAC **6** as well as PROTAC **8** showed comparable maximal degradation of PTK2 after 18 h and 72h days incubation (Supplemental figure 6). Taken together, this indicates that the both PROTACs **6** and **8** are suitable probes to further study the role of PTK2 in a broad range of tumour cell lines.

1  
2  
3 Reasoning that additional targeting of the scaffolding functions of PTK2 by PROTAC-  
4 mediated degradation might result in enhanced efficacy as compared to inhibition of its kinase  
5 activity, we next tested the effect of PROTAC-mediated PTK2 degradation on proliferation of  
6 the same HCC cell lines. Surprisingly, efficient depletion of PTK2 by both PROTACs (Table 3  
7 and Supplemental figures 2 and 3) did not affect proliferation of the tested cell lines more  
8 severely than the PTK2 inhibitor BI-4464 in standard culture conditions or in anchorage-  
9 independent growth assays (Table 3, Supplemental figures 4 and 5). Notably, sensitivity to  
10 genetic depletion of PTK2 has been described for several of the tested cell lines (Supplemental  
11 table 4). One explanation may be that effects on proliferation may require long-term depletion of  
12 PTK2. To further address this, we treated cell lines with reported high sensitivity to genetic  
13 depletion of PTK2<sup>36, 46</sup> (Supplemental table 4) for 21 days with either PROTAC **6** (BI-3663) or **8**  
14 (BI-0319) or the PTK2 inhibitor **1** (BI-4464). Despite the effective depletion of PTK2 even after  
15 21 days, we did not observe any pronounced anti-proliferative effects for any of the tested cell  
16 lines (Supplemental figure 6). Notably, CRISPR-based genetic validation in cultured HuH-1  
17 cells also resulted in a weak dependency on PTK2 (Supplemental figure 7). Taken together, these  
18 data questions the scaffolding function of PTK2 being required for *in vitro* proliferation of the  
19 tested cell lines beyond the effect of inhibition of its kinase activity. Nevertheless, our  
20 observations indicate that both probes can be used to effectively reduce PTK2 protein levels in  
21 long term experiments in cultured cells.  
22  
23  
24  
25  
26  
27  
28  
29  
30  
31  
32  
33  
34  
35  
36  
37  
38  
39  
40  
41  
42  
43  
44  
45  
46  
47  
48  
49  
50  
51  
52  
53  
54  
55  
56  
57  
58  
59  
60

**Table 3.** Degradation characteristics and effect on proliferation of BI-3663 (**6**) and BI-0319 (**8**) in HCC lines.

Cell line	BI-3663			BI-0319			BI-4464
	pDC <sub>50</sub>	D <sub>max</sub> [%]	pIC <sub>50</sub> (proliferation)	pDC <sub>50</sub>	D <sub>max</sub> [%]	pIC <sub>50</sub> (proliferation)	pIC <sub>50</sub> (proliferation)
SNU-387	7.6	90.0	<4.6	7.5	98.0	5.3	5.2
HUH-1	6.6	50.0	4.6	7.1	79.0	4.7	5.4
Hep3B2.1-7	7.9	96.0	4.6	6.2	59.0	5.2	5.3
HepG2	7.5	89.0	<4.6	6.2	65.0	<4.6	5.5
SK-Hep-1	7.5	89.0	5.8	6.9	87.0	5.1	5.2
HLF	6.4	30.0	<4.6	7.4	66.0	<4.6	5.4
SNU-398	8.5	95.0	<4.6	8.0	99.0	5.1	5.2
HUCCT1	7.9	90.0	<4.6	6.9	86.0	5.2	5.2
HLE	6.8	79.0	<4.6	7.6	85.0	5.0	5.1
HuH-7	7.3	93.0	<4.6	7.0	79.0	5.4	5.4
SNU-423	7.9	93.0	4.7	7.1	87.0	5.2	5.4

## Conclusion

We describe the development of two highly selective and functional PROTACs to degrade the PTK2 protein, a kinase of significant relevance to cancer research, in particular, in the area of hepatocellular carcinoma. Structure-guided conjugation of a highly selective PTK2 inhibitor BI-4464 to either a CRBN or VHL ligand via polyethylene glycol linkers led to the selective PTK2 degraders BI-0319 and BI-3663, respectively, using orthogonal E3 ligase binders. Both PROTACs were characterized with respect to *in vitro* PTK2 engagement, ligase dependence

1  
2  
3 selectivity (kinase inhibition as well as whole cell proteome) and degradation efficacy ( $DC_{50}$  and  
4  
5  $D_{max}$ ) in twelve cell lines (one lung cancer and eleven hepatocellular carcinoma cell lines). Both  
6  
7 PROTACs are highly selective E3 ligase-dependent PTK2 degraders and show overall  
8  
9 comparable potencies and efficacies of PTK2 degradation in the 12 cell tested lines. Whereas  
10  
11 PTK2 levels in cell lines such as SNU-398 were equally sensitive to treatment with both  
12  
13 PROTACs, other cell lines, such as Hep3B2.1-7 exhibited a more than ten-fold difference in  
14  
15 cellular potency. This difference in degradation efficacy in Hep3B2.1-7 cells was associated with  
16  
17 a higher degradation rate of BI-3663. Despite the efficient depletion of PTK2, treatment with  
18  
19 either PROTAC did not affect proliferation of the tested cell lines in either short or long term  
20  
21 assays in vitro (6 vs 21 days) beyond the effect achieved by a PTK2 kinase inhibitor. Taken  
22  
23 together, these data suggest that PROTACs **6** (BI-3663) and **8** (BI-0319) mediated PTK2  
24  
25 depletion is likely insufficient to affect proliferation in vitro under the conditions tested beyond  
26  
27 the effect of inhibition of its kinase activity. Nevertheless, both probes provide valuable tools to  
28  
29 effectively reduce PTK2 protein levels in experimental conditions that might be better suited to  
30  
31 reveal and differentiate between kinase- dependent and -independent functions of PTK2. BI-  
32  
33 3663, BI-0319 and its inactive control BI-4206 will be made available to all scientists via our  
34  
35 open innovation portal [opnMe](#).  
36  
37  
38  
39  
40  
41  
42  
43  
44  
45  
46  
47  
48  
49  
50  
51  
52  
53  
54  
55  
56  
57  
58  
59  
60

**EXPERIMENTAL SECTION**

**Chemistry. Synthesis.** Unless otherwise indicated, all reactions were carried out in standard commercially available glassware using standard synthetic chemistry methods. Air-sensitive and moisture-sensitive reactions were performed under an atmosphere of dry nitrogen or argon with dried glassware. Commercial starting materials were used without further purification. Solvents used for reactions were of commercial “dry”- or “extra-dry” or “analytical” grade. All other solvents used were reagent grade.

The thin layer chromatography is carried out on ready-made silica gel 60 TLC plates on glass (with fluorescence indicator F-254) made by Merck. The preparative high pressure chromatography (RP-HPLC) is carried out on Gilson systems with columns made by Waters (names: Sunfire™ Prep C18, OBD™ 10 μm, 50x150 mm or XBridge™ Prep C18, OBD™ 10 μm, 50x150 mm) and YMC (names: Actus-Triart Prep C18, 5 μm, 30x50 mm). Different gradients of MeCN/H<sub>2</sub>O are used to elute the compounds, for acidic conditions 0.1 % HCOOH is added to the water. For the chromatography under basic conditions the water is made alkaline as follows: 5 mL NH<sub>4</sub>HCO<sub>3</sub> solution (158 g in 1 L H<sub>2</sub>O) and 2 mL NH<sub>3</sub> (28 % in H<sub>2</sub>O) are replenished to 1 L with H<sub>2</sub>O.

All compounds had a purity >95% according to HPLC and NMR analysis acquired with the systems and parameters stated in the following. HPLC samples were analyzed on an Agilent 1200 series LC system coupled with an Agilent 6140 mass spectrometer. Purity was determined via UV detection with a bandwidth of 170nm in the range from 230-400nm. LC parameters were as follows: Waters Xbridge C18 column, 2.5μm particle size, 2.1 x 20mm. Total run time 3.1 minutes, flow 1ml/min, column temperature 60°C and 5μl injections. Solvent A (20mM



1  
2  
3 NH<sub>4</sub>HCO<sub>3</sub>/ NH<sub>3</sub> pH 9), solvent B (MS grade acetonitrile). Start 10% B, gradient 10% - 95% B  
4  
5 from 0.0 - 1.5min, 95% B from 1.5 - 2.0min, gradient 95% - 10% B from 2.0 – 2.1min.  
6  
7

8  
9 NMR experiments were recorded on a Bruker Avance HD 500 MHz spectrometer equipped  
10  
11 with a TCI cryoprobe at 298 K. Samples were dissolved in 600 μL DMSO-d<sub>6</sub> and TMS was  
12  
13 added as an internal standard. 1D <sup>1</sup>H spectra were acquired with 30° excitation pulses and an  
14  
15 interpulse delay of 4.2 sec with 64k data points and 20 ppm sweep width. 1D <sup>13</sup>C spectra were  
16  
17 acquired with broadband composite pulse decoupling (WALTZ16) and an interpulse delay of 3.3  
18  
19 sec with 64 k data points and a sweep width of 240 ppm. Processing and analysis of 1D spectra  
20  
21 was performed with Bruker Topspin 3.2 software. No zero filling was performed and spectra  
22  
23 were manually integrated after automatic baseline correction. Chemical shifts are reported in  
24  
25 ppm on the δ scale.  
26  
27  
28  
29

30  
31 HSQC spectra were recorded on all samples to aid the interpretation of the data and to identify  
32  
33 signals hidden underneath solvent peaks. Spectra were acquired with sweep widths obtained by  
34  
35 automatic sweep width detection from 1D reference spectra in the direct dimension with 1k  
36  
37 datapoints and with 210 ppm, and 256 datapoints in the indirect dimension.  
38  
39

40  
41 For HRMS a LTQ Orbitrap XL (Thermo Scientific) coupled with a Triversa Nanomate  
42  
43 Nanospray ion source (ADVION Bioscience Inc.) was used.  
44

45  
46 **3-methoxy-4-({4-[(3-oxo-2,3-dihydro-1H-inden-4-yl)oxy]-5-(trifluoromethyl)pyrimidin-2-**  
47  
48 **yl}amino)benzoic acid (1a).** 4-{{[4-chloro-5-(trifluoromethyl)pyrimidin-2-yl]amino}-3-  
49  
50 methoxybenzoic acid (**4**<sup>47</sup>, 1.00g, 1eq) and 7-hydroxy-2,3-dihydro-1H-inden-1-one (879 mg, 2  
51  
52 eq) were taken up in dioxane (10 mL), then Cs<sub>2</sub>CO<sub>3</sub> (4.686 g, 5 eq) was added. The reaction  
53  
54 mixture was stirred at 80°C for 16 h. The reaction mixture was diluted with H<sub>2</sub>O and acetonitrile  
55  
56  
57  
58  
59  
60

1  
2  
3 and concentrated under reduced pressure. The residue was purified by preparative RP-HPLC  
4 under basic conditions using MeCN/H<sub>2</sub>O as eluents in a gradient from 20:80 to 65:35 over 12  
5 min. (column: XBridge™ Prep C18, OBD™ 10 μm, 50x150 mm; flow: 110 mL/min). Product  
6 containing fractions were freeze dried to give 3-methoxy-4-({4-[(3-oxo-2,3-dihydro-1*H*-inden-4-  
7 yl)oxy]-5-(trifluoromethyl)pyrimidin-2-yl}amino)benzoic acid (**1a**, 1.03 g, 78% yield) as brown  
8 solid. <sup>1</sup>H NMR (500 MHz, DMSO-*d*<sub>6</sub>) δ = 12.85 (br s, 1H), 8.86 (s, 1H), 8.74 (s, 1H), 7.80 (t,  
9 *J*=7.88 Hz, 1H), 7.60 (d, *J*=7.88 Hz, 1H), 7.41 (d, *J*=0.95 Hz, 1H), 7.32 (br d, *J*=1.00 Hz, 1H),  
10 7.24 (d, *J*=7.88 Hz, 1H), 7.15 (br d, *J*=1.00 Hz, 1H), 3.80 (s, 3H), 3.05-3.17 (m, 2H), two protons  
11 under DMSO. <sup>13</sup>C NMR (125 MHz, DMSO-*d*<sub>6</sub>) δ = 203.4, 167.3, 166.4, 161.0, 158.4, 157.8,  
12 149.7, 148.0, 137.0, 131.7, 128.9, 126.5, 125.5, 121.8, 121.1, 123.9, 120.4, 111.7, 101.5, 56.3,  
13 36.7, 25.8. HRMS (*m/z*): [M+H]<sup>+</sup> calculated for C<sub>22</sub>H<sub>16</sub>F<sub>3</sub>N<sub>3</sub>O<sub>5</sub>, 459.10421; found, 459.10411.  
14 HPLC-MS <sup>t</sup>R = 1.00 min.

15  
16  
17  
18  
19  
20  
21  
22  
23  
24  
25  
26  
27  
28  
29  
30  
31  
32 **3-methoxy-N-(1-methylpiperidin-4-yl)-4-({4-[(3-oxo-2,3-dihydro-1*H*-inden-4-yl)oxy]-5-**  
33 **(trifluoromethyl)pyrimidin-2-yl}amino)benzamide (**1**, BI-4464).** In a glass vial, 3-methoxy-4-  
34 ({4-[(3-oxo-2,3-dihydro-1*H*-inden-4-yl)oxy]-5-(trifluoromethyl)pyrimidin-2-yl}amino)benzoic  
35 acid (**1a**, 100 mg, 1 eq) was dissolved in DMF (1 mL). DIPEA (86 μl, 3 eq) and HATU (114 mg,  
36 1.5 eq) were added. After the reaction mixture was stirred at rt for 5 min, 1-methylpiperidin-4-  
37 amine (46 mg, 52 μl, 2 eq) was added. The mixture was stirred at rt for 2 h. The reaction mixture  
38 was diluted with MeCN and H<sub>2</sub>O and filtered through a syringe filter prior to purification *via* RP-  
39 HPLC under basic conditions using MeCN/H<sub>2</sub>O as eluents in a gradient from 30:70 to 98:2 over  
40 8 min (column: YMC Actus-Triart Prep C18, 5 μm, 30x50 mm; flow: 50 mL/min). Product  
41 containing fractions were freeze dried to give 3-methoxy-*N*-(1-methylpiperidin-4-yl)-4-({4-[(3-  
42 oxo-2,3-dihydro-1*H*-inden-4-yl)oxy]-5-(trifluoromethyl)pyrimidin-2-yl}amino)benzamide (**1**,  
43  
44  
45  
46  
47  
48  
49  
50  
51  
52  
53  
54  
55  
56  
57  
58  
59  
60

1  
2  
3 **(BI-4464)**, 83 mg, 75% yield) as off-white lyophilizate. <sup>1</sup>H NMR (500 MHz, DMSO-*d*<sub>6</sub>) δ = 8.83  
4 (br s, 1H), 8.69 (s, 1H), 8.13 (d, *J*=7.57 Hz, 1H), 7.77 (dd, *J*=7.57, 7.88 Hz, 1H), 7.55 (d, *J*=7.57  
5 Hz, 1H), 7.38 (d, *J*=0.95 Hz, 1H), 7.22 (d, *J*=7.88 Hz, 1H), 7.27 (br s, 1H), 7.12 (br s, 1H), 3.78  
6 (s, 3H), 3.66-3.75 (m, 1H), 3.04-3.15 (m, 2H), 2.78 (br d, *J*=11.35 Hz, 2H), 2.16 (s, 3H), 1.85-  
7 1.98 (m, 2H), 1.69-1.80 (m, 2H), 1.49-1.65 (m, 2H), two protons under DMSO. <sup>13</sup>C NMR (125  
8 MHz, DMSO-*d*<sub>6</sub>) δ = 201.3, 164.2, 163.2, 159.1, 156.2, 155.7, 148.0, 145.8, 134.8, 128.8, 127.8,  
9 126.8, 123.3, 118.8, 121.9, 117.5, 108.1, 99.0, 54.2, 53.0, 45.0, 44.4, 34.6, 29.9, 23.7, one carbon  
10 not detected. HRMS (*m/z*): [M+H]<sup>+</sup> calculated for C<sub>28</sub>H<sub>28</sub>F<sub>3</sub>N<sub>5</sub>O<sub>4</sub>, 555.20934; found, 555.20824.  
11 HPLC-MS <sup>t</sup>R = 1.39 min.  
12  
13  
14  
15  
16  
17  
18  
19  
20  
21  
22  
23

24  
25 **3-{2-[2-(2-azidoethoxy)ethoxy]ethoxy}-N-[2-(2,6-dioxopiperidin-3-yl)-1,3-dioxo-2,3-**  
26 **dihydro-1H-isoindol-4-yl]propanamide (5a)**. In a 50 mL round-bottom flask, 4-amino-2-(2,6-  
27 dioxo-3-piperidyl)isoindoline-1,3-dione (500 mg, 1 eq) was dissolved in DMF (5 mL) and  
28 cooled to 0°C in an ice bath. 3-{2-[2-(2-azidoethoxy)ethoxy]ethoxy}propanoic acid (905 mg, 2  
29 eq) was added dropwise. Then *N*-propylphosphonic acid anhydride, cyclic trimer (7.0 g, 6.5 mL,  
30 6 eq) and pyridine (1.5 mL, 10 eq) were added. The mixture was stirred at 80°C for 3h. The  
31 reaction mixture was diluted with ACN/H<sub>2</sub>O. The solution was filtered through a syringe filter  
32 and purified by preparative RP-HPLC under basic conditions using MeCN/H<sub>2</sub>O as eluents in a  
33 gradient from 10:90 to 60:40 over 9 min. (column: XBridge™ Prep C18, OBD™ 10 μm, 50x150  
34 mm; flow: 150 mL/min). Product containing fractions were freeze dried to give 3-{2-[2-(2-  
35 azidoethoxy)ethoxy]ethoxy}-*N*-[2-(2,6-dioxopiperidin-3-yl)-1,3-dioxo-2,3-dihydro-1*H*-isoindol-  
36 4-yl]propanamide (**5a**, 697 mg, 76% yield) as yellow lyophilizate. <sup>1</sup>H NMR (500 MHz, DMSO-  
37 *d*<sub>6</sub>) δ = 11.15 (s, 1H), 9.88 (s, 1H), 8.54 (d, *J*=8.31 Hz, 1H), 7.83 (dd, *J*=7.26, 8.31 Hz, 1H), 7.62  
38 (d, *J*=7.26 Hz, 1H), 5.14 (dd, *J*=5.52, 12.77 Hz, 1H), 3.74 (t, *J*=5.83 Hz, 2H), 3.52-3.61 (m, 6H),  
39  
40  
41  
42  
43  
44  
45  
46  
47  
48  
49  
50  
51  
52  
53  
54  
55  
56  
57  
58  
59  
60

1  
2  
3 3.47-3.52 (m, 4H), 3.34-3.37 (m, 2H), 2.84-2.96 (m, 1H), 2.70 (t,  $J=5.99$  Hz, 2H), 2.53-2.66 (m,  
4  
5 2H), 2.00-2.12 (m, 1H).  $^{13}\text{C}$  NMR (125 MHz, DMSO- $d_6$ )  $\delta$  = 173.2, 170.9, 170.2, 168.1, 167.1,  
6  
7 136.9, 136.6, 131.9, 126.5, 118.7, 117.1, 70.2, 70.2, 70.1, 70.1, 69.7, 66.6, 50.4, 49.4, 38.0, 31.4,  
8  
9 22.4. HRMS ( $m/z$ ):  $[\text{M}+\text{H}]^+$  calculated for  $\text{C}_{22}\text{H}_{26}\text{N}_6\text{O}_8$ , 502.18121; found, 502.18114. HPLC-  
10  
11 MS  $t_R$  = 1.05 min.  
12  
13  
14

15  
16 **3-{2-[2-(2-aminoethoxy)ethoxy]ethoxy}-N-[2-(2,6-dioxopiperidin-3-yl)-1,3-dioxo-2,3-**  
17  
18 **dihydro-1H-isoindol-4-yl]propanamide (5b).** In a Parr-reactor 3-{2-[2-(2-  
19  
20 azidoethoxy)ethoxy]ethoxy}-N-[2-(2,6-dioxopiperidin-3-yl)-1,3-dioxo-2,3-dihydro-1H-isoindol-  
21  
22 4-yl]propanamide (**5a**, 190 mg, 1 eq) was dissolved in methanol (5 mL) and Pd/C (10%, 40 mg,  
23  
24 0.1 eq) was added. The reactor was flushed with  $\text{N}_2$  and filled with  $\text{H}_2$  (6 bar). The reaction  
25  
26 mixture was stirred at rt for 3 h. A spoon of celite was added to the reaction mixture, the catalyst  
27  
28 was filtered off through a celite pad and rinsed with DCM and MeOH. The filtrate was  
29  
30 concentrated under reduced pressure. 3-{2-[2-(2-aminoethoxy)ethoxy]ethoxy}-N-[2-(2,6-  
31  
32 dioxopiperidin-3-yl)-1,3-dioxo-2,3-dihydro-1H-isoindol-4-yl]propanamide (**5b**, 162 mg, 90%  
33  
34 yield) was obtained as yellow resin. The product was taken to the next step without further  
35  
36 purification.  $^1\text{H}$  NMR (500 MHz, DMSO- $d_6$ )  $\delta$  = ppm 9.89 (br s, 1 H), 8.54 (d,  $J=8.20$  Hz, 1 H),  
37  
38 8.36 (s, 1 H), 7.84 (dd,  $J=8.20, 7.25$  Hz, 1 H), 7.62 (br d,  $J=7.25$  Hz, 1 H), 5.14 (dd,  $J=12.93,$   
39  
40 5.36 Hz, 1 H), 3.71 - 3.77 (m, 2 H), 3.45 - 3.60 (m, overlapped), 2.85 - 2.96 (m, 2 H), 2.82 (br t,  
41  
42  $J=5.36$  Hz, 2 H), 2.71 (br t,  $J=5.83$  Hz, 2 H), 2.02 - 2.11 (m, 1 H).  $^{13}\text{C}$  NMR (125 MHz, DMSO-  
43  
44  $d_6$ )  $\delta$  = 173.3, 170.9, 170.3, 168.1, 167.1, 136.9, 136.7, 131.9, 126.5, 118.8, 117.2, 70.2, 70.1,  
45  
46 70.1, 70.0, 69.2, 66.6, 49.4, 39.8, 38.0, 31.4, 22.4. HRMS ( $m/z$ ):  $[\text{M}+\text{H}]^+$  calculated for  
47  
48  $\text{C}_{22}\text{H}_{28}\text{N}_4\text{O}_8$ , 476.19071; found, 476.19041. HPLC-MS  $t_R$  = 0.81 min.  
49  
50  
51  
52  
53  
54  
55  
56  
57  
58  
59  
60

**N-[2-(2,6-dioxopiperidin-3-yl)-1,3-dioxo-2,3-dihydro-1H-isoindol-4-yl]-3-{2-[2-(2-{[3-methoxy-4-({4-[(3-oxo-2,3-dihydro-1H-inden-4-yl)oxy]-5-(trifluoromethyl)pyrimidin-2-yl}amino)phenyl]formamido}ethoxy)ethoxy]ethoxy}propanamide (6, BI-3663).** In a glass vial, 3-methoxy-4-({4-[(3-oxo-2,3-dihydro-1H-inden-4-yl)oxy]-5-(trifluoromethyl)pyrimidin-2-yl}amino)benzoic acid (**2**, 170 mg, 1 eq) was dissolved in DMF (2 mL). DIPEA (150  $\mu$ L, 3 eq) and HATU (155 mg, 1.2 eq) were added. The reaction mixture was stirred at rt for 5 min, then 3-{2-[2-(2-aminoethoxy)ethoxy]ethoxy}-*N*-[2-(2,6-dioxopiperidin-3-yl)-1,3-dioxo-2,3-dihydro-1H-isoindol-4-yl]propanamide (**5b**, 162 mg, 1eq) was added. The mixture was stirred at rt overnight. The reaction mixture was diluted with MeCN and H<sub>2</sub>O and filtered through a syringe filter prior to purification *via* RP-HPLC under acidic conditions using MeCN/H<sub>2</sub>O as eluents in a gradient from 30:70 to 98:2 over 8 min (column: YMC Actus-Triart Prep C18, 5  $\mu$ m, 30x50 mm; flow: 50 mL/min). Product containing fractions were freeze dried to give *N*-[2-(2,6-dioxopiperidin-3-yl)-1,3-dioxo-2,3-dihydro-1H-isoindol-4-yl]-3-{2-[2-(2-{[3-methoxy-4-({4-[(3-oxo-2,3-dihydro-1H-inden-4-yl)oxy]-5-(trifluoromethyl)pyrimidin-2-yl}amino)phenyl]formamido}ethoxy)ethoxy]ethoxy}propanamide (**6 (BI-3663)**, 32 mg, 10% yield) as off-white lyophilizate. <sup>1</sup>H NMR (500 MHz, DMSO-*d*<sub>6</sub>)  $\delta$  = 11.13 (br s, 1H), 9.86 (s, 1H), 8.79 (br s, 1H), 8.70 (s, 1H), 8.53 (d, *J*=8.51 Hz, 1H), 8.43 (t, *J*=5.52 Hz, 1H), 7.81 (dd, *J*=7.25, 8.51 Hz, 1H), 7.77 (t, *J*=7.88 Hz, 1H), 7.60 (d, *J*=7.25 Hz, 1H), 7.56 (d, *J*=7.88 Hz, 1H), 7.40 (s, 1H), 7.21 (d, *J*=7.88 Hz, 1H), 7.25 (br s, 1H), 7.10 (br s, 1H), 5.14 (dd, *J*=5.52, 12.77 Hz, 1H), 3.78 (s, 3H), 3.71 (t, *J*=5.99 Hz, 2H), 3.43-3.61 (m, 10H), 3.36-3.41 (m, 2H), 3.07-3.15 (m, 2H), 2.84-2.95 (m, 1H), 2.68 (t, *J*=5.99 Hz, 2H), 2.52-2.65 (m, 2H), 2.02-2.11 (m, 1H), two protons under DMSO. <sup>13</sup>C NMR (125 MHz, DMSO-*d*<sub>6</sub>)  $\delta$  = 203.4, 173.2, 170.9, 170.3, 168.1, 167.1, 166.4, 165.9, 161.1, 158.3, 157.8, 149.9, 147.9, 136.9, 136.9, 136.6, 131.9, 130.4, 130.0,

1  
2  
3 128.9, 126.4, 125.5, 120.9, 124.0, 119.5, 118.7, 117.1, 110.2, 101.2, 70.2, 70.2, 70.1, 70.0, 69.5,  
4  
5 66.6, 56.3, 49.4, 39.6, 38.0, 36.8, 31.4, 25.8, 22.4, one carbon not detected. HRMS (*m/z*):  
6  
7 [M+H]<sup>+</sup> calculated for C<sub>44</sub>H<sub>42</sub>F<sub>3</sub>N<sub>7</sub>O<sub>12</sub>, 917.28435; found, 917.28471. HPLC-MS <sup>t</sup>R = 1.35 min.  
8  
9

10  
11 **(2*S*,4*R*)-1-[(2*S*)-2-(2-{2-[2-(2-azidoethoxy)ethoxy]ethoxy}acetamido)-3,3-dimethyl-**  
12  
13 **butanoyl]-4-hydroxy-*N*-{[4-(4-methyl-1,3-thiazol-5-yl)phenyl]methyl}pyrrolidine-2-**  
14  
15 **carboxamide (7a).** (2*S*,4*R*)-1-[(2*S*)-2-amino-3,3-dimethyl-butanoyl]-4-hydroxy-*N*-[[4-(4-  
16 methylthiazol-5-yl)phenyl]methyl]pyrrolidine-2-carboxamide hydrochloride (**2**, 1.000 g, 1 eq)  
17 was dissolved in DMF (5 mL). HATU (855 mg, 1.05 eq) and DIPEA (1.28 mL, 3.5 eq) were  
18 added. The reaction mixture was stirred for 15 min, then 2-[2-[2-(2-  
19 azidoethoxy)ethoxy]ethoxy]acetic acid (524 mg, 1.05 eq) was added. The reaction mixture was  
20 stirred at rt for 1 h. The reaction mixture was diluted with EtOAc and washed with a saturated  
21 solution of NaHCO<sub>3</sub> and then with brine. The organic layer is dried over MgSO<sub>4</sub> and evaporated.  
22 The residue was purified *via* RP-HPLC under acidic conditions using MeCN/H<sub>2</sub>O as eluents in a  
23 gradient from 10:90 to 98:2 over 10 min (column: Sunfire™ Prep C18, OBD™ 10 μm, 50x150  
24 mm; flow: 120 mL/min). Product containing fractions were freeze dried to give (2*S*,4*R*)-1-[(2*S*)-  
25 2-(2-{2-[2-(2-azidoethoxy)ethoxy]ethoxy}acetamido)-3,3-dimethylbutanoyl]-4-hydroxy-*N*-{[4-  
26 (4-methyl-1,3-thiazol-5-yl)phenyl]methyl}pyrrolidine-2-carboxamide (**7a**, 870 mg, 63% yield).  
27 <sup>1</sup>H NMR (500 MHz, DMSO-*d*<sub>6</sub>) δ = 8.98 (s, 1H), 8.60 (t, *J*=5.99 Hz, 1H), 7.35-7.47 (m, 5H),  
28 4.67-5.61 (m, 1H), 4.57 (d, *J*=9.77 Hz, 1H), 4.32-4.48 (m, 3H), 4.21-4.29 (m, 1H), 3.97 (s, 2H),  
29 3.64-3.69 (m, 1H), 3.53-3.64 (m, 12H), 2.44 (s, 3H), 2.02-2.09 (m, 1H), 1.85-1.94 (m, 1H), 0.93-  
30 0.96 (m, 8H), 0.94 (s, 1H), one proton under water. <sup>13</sup>C NMR (125 MHz, DMSO-*d*<sub>6</sub>) δ = 172.2,  
31 169.6, 169.1, 152.0, 148.2, 139.9, 131.6, 130.2, 129.2, 127.9, 70.9, 70.4, 70.2, 70.1, 70.1, 69.7,  
32  
33  
34  
35  
36  
37  
38  
39  
40  
41  
42  
43  
44  
45  
46  
47  
48  
49  
50  
51  
52  
53  
54  
55  
56  
57  
58  
59  
60

69.3, 59.2, 57.0, 56.1, 50.4, 42.1, 38.4, 36.2, 26.6, 16.4. HRMS ( $m/z$ ):  $[M+H]^+$  calculated for  $C_{30}H_{43}N_7O_7S$ , 645.29447; found, 645.29442. HPLC-MS  $t_R = 1.16$  min.

**(2S,4R)-1-[(2S)-2-(2-{2-[2-(2-aminoethoxy)ethoxy]ethoxy}acetamido)-3,3-dimethylbutanoyl]-4-hydroxy-N-{[4-(4-methyl-1,3-thiazol-5-yl)phenyl]methyl}pyrrolidine-2-carboxamide (7b).** (2S,4R)-1-[(2S)-2-(2-{2-[2-(2-azidoethoxy)ethoxy]ethoxy}acetamido)-3,3-dimethylbutanoyl]-4-hydroxy-N-{[4-(4-methyl-1,3-thiazol-5-yl)phenyl]methyl}pyrrolidine-2-carboxamide (**7a**, 1.475 g, 1 eq) was dissolved in MeOH (10 mL), Pd/C (250 mg, 10 %) was added and the mixture was hydrogenated (5 bar  $H_2$  pressure) at rt for 2.5 h. The catalyst was filtered off and the filtrate was purified *via* RP-HPLC under basic conditions using MeCN/ $H_2O$  as eluents in a gradient from 10:90 to 90:10 over 10 min. (column: XBridge™ Prep C18, OBD™ 10  $\mu$ m, 50x150 mm; flow: 140 mL/min). Product containing fractions were freeze dried to give (2S,4R)-1-[(2S)-2-(2-{2-[2-(2-aminoethoxy)ethoxy]ethoxy}acetamido)-3,3-dimethylbutanoyl]-4-hydroxy-N-{[4-(4-methyl-1,3-thiazol-5-yl)phenyl]methyl}pyrrolidine-2-carboxamide (**7b**, 1.166 g, 82% yield).  $^1H$  NMR (500 MHz, DMSO- $d_6$ )  $\delta = 9.00$  (s, 1H), 8.64 (t,  $J=6.00$  Hz, 1H), 7.37-7.49 (m, 5H), 5.17 (br s, 1H), 4.58 (br d,  $J=9.46$  Hz, 1H), 4.21-4.48 (m, 4H), 3.99 (s, 2H), 3.65-3.71 (m, 1H), 3.51-3.65 (m, 9H), 3.46 (t,  $J=5.50$  Hz, 1H), 2.79 (t,  $J=5.67$  Hz, 1H), 2.45 (s, 3H), 2.02-2.11 (m, 1H), 1.86-1.96 (m, 1H), 0.95 (s, 9H), two protons not detected ( $NH_2$ ).  $^{13}C$  NMR (125 MHz, DMSO- $d_6$ )  $\delta = 172.2, 169.6, 169.1, 152.0, 148.2, 139.9, 131.6, 130.2, 129.2, 127.9, 70.9, 70.4, 70.2, 70.1, 70.1, 70.0, 69.3, 59.2, 57.1, 56.2, 42.1, 38.4, 36.2, 26.7, 16.4$ , one carbon not detected. HRMS ( $m/z$ ):  $[M+H]^+$  calculated for  $C_{30}H_{45}N_5O_7S$ , 619.30397; found, 619.30333. HPLC-MS  $t_R = 1.00$  min.

**(2S,4R)-4-hydroxy-1-[(2S)-2-(2-{2-[2-(2-{[3-methoxy-4-({4-[(3-oxo-2,3-dihydro-1H-inden-4-yl)oxy]-5-(trifluoromethyl)pyrimidin-2-yl}amino)phenyl]formamido}ethoxy)**

1  
2  
3 **ethoxy]ethoxy}acetamido)-3,3-dimethylbutanoyl]-N-{[4-(4-methyl-1,3-thiazol-5-**  
4  
5 **yl)phenyl]methyl}pyrrolidine-2-carboxamide (8, BI-0319).** In a 50 mL round-bottom flask, 3-  
6 methoxy-4-({4-[(3-oxo-2,3-dihydro-1*H*-inden-4-yl)oxy]-5-(trifluoromethyl)pyrimidin-2-  
7  
8 yl}amino)benzoic acid (**2**, 111 mg, 1 eq) was dissolved in DMF (3 mL). DIPEA (96  $\mu$ L, 3 eq) and  
9  
10 HATU (101 mg; 266  $\mu$ mol; 1.2 eq) were added. The reaction mixture was stirred at rt for 5 min,  
11  
12 then (2*S*,4*R*)-1-[(2*S*)-2-[[2-[2-[2-(2-aminoethoxy)ethoxy] ethoxy]acetyl]amino]-3,3-dimethyl-  
13  
14 butanoyl]-4-hydroxy-*N*-[[4-(4-methylthiazol-5-yl)phenyl]methyl]pyrrolidine-2-carboxamide (**7b**,  
15  
16 150 mg, 1 eq) was added. The mixture was stirred at rt for 24h. The reaction mixture was diluted  
17  
18 with MeCN and H<sub>2</sub>O and filtered through a syringe filter prior to purification *via* RP-HPLC  
19  
20 under basic conditions using MeCN/H<sub>2</sub>O as eluents in a gradient from 25:75 to 90:10 over 9  
21  
22 min. (column: XBridge™ Prep C18, OBD™ 10  $\mu$ m, 50x150 mm; flow: 150 mL/min). The  
23  
24 product containing fractions were pooled and freeze-dried to give (2*S*,4*R*)-4-hydroxy-1-[(2*S*)-2-  
25  
26 (2-{{2-[2-(2-{{3-methoxy-4-({4-[(3-oxo-2,3-dihydro-1*H*-inden-4-yl)oxy]-5-  
27  
28 (trifluoromethyl)pyrimidin-2-yl}amino)phenyl]formamido}ethoxy)ethoxy]ethoxy}acetamido)-  
29  
30 3,3-dimethylbutanoyl]-*N*-{{4-(4-methyl-1,3-thiazol-5-yl)phenyl]methyl}pyrrolidine-2-  
31  
32 carboxamide (**8 (BI-0319)**, 81 mg, 34% yield) as colorless lyophilizate. <sup>1</sup>H NMR (500 MHz,  
33  
34 DMSO-*d*<sub>6</sub>)  $\delta$  = 8.97 (s, 1H), 8.80 (br s, 1H), 8.70 (s, 1H), 8.59 (t, *J*=5.99 Hz, 1H), 8.46 (t, *J*=5.67  
35  
36 Hz, 1H), 7.77 (dd, *J*=7.57, 7.88 Hz, 1H), 7.56 (d, *J*=7.57 Hz, 1H), 7.35-7.46 (m, 6H), 7.21 (d,  
37  
38 *J*=7.88 Hz, 1H), 7.23 (br s, 1H), 7.11 (br s, 1H), 5.15 (d, *J*=3.47 Hz, 1H), 4.56 (d, *J*=9.77 Hz,  
39  
40 1H), 4.20-4.48 (m, 4H), 3.96 (s, 2H), 3.77 (s, 3H), 3.36-3.71 (m, 16H), 3.06-3.15 (m, 2H), 2.43  
41  
42 (s, 3H), 2.00-2.10 (m, 1H), 1.85-1.94 (m, 1H), 0.93 (s, 9H). <sup>13</sup>C NMR (125 MHz, DMSO-*d*<sub>6</sub>)  $\delta$  =  
43  
44 203.4, 172.2, 169.6, 169.1, 166.4, 166.0, 161.1, 158.3, 157.8, 151.9, 150.0, 148.2, 147.9, 139.9,  
45  
46 136.9, 131.6, 130.4, 130.2, 130.0, 129.1, 128.9, 127.9, 125.5, 121.0, 124.0, 119.5, 110.2, 101.3,  
47  
48  
49  
50  
51  
52  
53  
54  
55  
56  
57  
58  
59  
60



1  
2  
3 101.1, 70.9, 70.3, 70.2, 70.1, 70.0, 69.5, 69.3, 59.2, 57.0, 56.3, 56.2, 42.1, 38.4, 36.8, 36.2, 26.6,  
4  
5 25.8, 16.4. HRMS ( $m/z$ ):  $[M+H]^+$  calculated for  $C_{52}H_{59}F_3N_8O_{11}S$ , 1060.39761; found,  
6  
7 1060.39604. HPLC-MS  $t_R$  = 1.35 min.

10  
11 **(2S,4S)-1-[(2S)-2-(2-{2-[2-(2-azidoethoxy)ethoxy]ethoxy}acetamido)-3,3-**  
12  
13 **dimethylbutanoyl]-4-hydroxy-N-[[4-(4-methyl-1,3-thiazol-5-yl)phenyl]methyl]pyrrolidine-**  
14  
15 **2-carboxamide (10a).** In a glass vial 2-[2-[2-(2-azidoethoxy) ethoxy] ethoxy]acetic acid (**9**, 569  
16 mg, 1.05 eq) was dissolved in DMF (1 mL) and DIPEA (768  $\mu$ l, 2 eq). HATU (1.324 g 1.5 eq)  
17 and (2S,4S)-1-[(2S)-2-amino-3,3-dimethylbutanoyl]-4-hydroxy-N-[[4-(4-methyl-1,3-thiazol-5-  
18 yl)phenyl]methyl]pyrrolidine-2-carboxamide (1.000 g, 1 eq) were added. The mixture was  
19 stirred at rt for 2 h. The reaction mixture was diluted with EtOAc and washed with a saturated  
20 solution of  $NaHCO_3$  then with brine. The organic layer was evaporated and the residue was  
21 dissolved in MeOH and purified *via* RP-HPLC under acidic conditions using MeCN/ $H_2O$  as  
22 eluents in a gradient from 15:85 to 98:2 over 10 min (column: Sunfire™ Prep C18, OBD™ 10  
23  $\mu$ m, 50x150 mm; flow: 120 mL/min). Product containing fractions were freeze dried to give  
24 (2S,4S)-1-[(2S)-2-(2-{2-[2-(2-azidoethoxy)ethoxy]ethoxy}acetamido)-3,3-dimethylbutanoyl]-4-  
25 hydroxy-N-[[4-(4-methyl-1,3-thiazol-5-yl)phenyl]methyl]pyrrolidine-2-carboxamide (**10a**, 700  
26 mg, 47% yield).  $^1H$  NMR (500 MHz, DMSO- $d_6$ )  $\delta$  = 8.99 (s, 1H), 8.67 (t,  $J$ =5.99 Hz, 1H), 7.36-  
27 7.43 (m, 5H), 5.36 (br s, 1H), 4.52 (d,  $J$ =9.14 Hz, 1H), 4.18-4.47 (m, 4H), 3.95 (s, 2H), 3.84-3.91  
28 (m, 1H), 3.51-3.64 (m, 11H), 3.43-3.48 (m, 1H), 2.44 (s, 3H), 2.29-2.39 (m, 1H), 1.68-1.79 (m,  
29 1H), 0.96 (s, 9H), one proton under water.  $^{13}C$  NMR (125 MHz, DMSO- $d_6$ )  $\delta$  = 172.7, 169.8,  
30 169.3, 152.0, 148.2, 139.6, 131.6, 130.2, 129.2, 127.9, 70.9, 70.3, 70.2, 70.1, 70.0, 69.7, 69.5,  
31 59.0, 56.3, 56.1, 50.4, 42.3, 37.4, 35.6, 26.6, 16.4. HRMS ( $m/z$ ):  $[M+H]^+$  calculated for  
32  $C_{30}H_{43}N_7O_7S$ , 645.29447; found, 645.29368. HPLC-MS  $t_R$  = 1.18 min.  
33  
34  
35  
36  
37  
38  
39  
40  
41  
42  
43  
44  
45  
46  
47  
48  
49  
50  
51  
52  
53  
54  
55  
56  
57  
58  
59  
60

**(2S,4S)-1-[(2S)-2-(2-{2-[2-(2-aminoethoxy)ethoxy]ethoxy}acetamido)-3,3-dimethylbutanoyl]-4-hydroxy-N-{[4-(4-methyl-1,3-thiazol-5-yl)phenyl]methyl}pyrrolidine-2-carboxamide (10b).** In a Parr-reactor (2S,4S)-1-[(2S)-2-(2-{2-[2-(2-azidoethoxy)ethoxy]ethoxy}acetamido)-3,3-dimethylbutanoyl]-4-hydroxy-N-{[4-(4-methyl-1,3-thiazol-5-yl)phenyl]methyl}pyrrolidine-2-carboxamide (**10a**, 153 mg, 1 eq) was dissolved in methanol (5 mL) and Pd/C (10%, 25 mg, 0.1 eq) was added. The reactor was flushed with N<sub>2</sub> and filled with H<sub>2</sub> (6 bar). The reaction mixture was allowed to at rt for 3 h. A spoon of celite was added to the reaction mixture, the catalyst was filtered off through a pad of celite and rinsed with DCM and MeOH. The filtrate was concentrated under reduced pressure. (2S,4S)-1-[(2S)-2-(2-{2-[2-(2-aminoethoxy)ethoxy]ethoxy}acetamido)-3,3-dimethylbutanoyl]-4-hydroxy-N-{[4-(4-methyl-1,3-thiazol-5-yl)phenyl]methyl}pyrrolidine-2-carboxamide (**10b**, 144 mg, 98% yield) was obtained as colorless resin. The product was taken to the next step without further purification. <sup>1</sup>H NMR (500 MHz, DMSO-d<sub>6</sub>) δ = 8.99 (s, 1H), 8.72 (br t, *J*=5.83 Hz, 1H), 8.36 (br s, 1H), 7.40 (s, 4H), 5.32 (br s, 1H), 4.52 (d, *J*=9.14 Hz, 1H), 4.18-4.45 (m, 4H), 3.96 (s, 2H), 3.86-3.91 (m, 1H), 3.42-3.62 (m, 11H), 2.82 (br s, 2H), 2.44 (s, 3H), 2.31-2.38 (m, 1H), 1.68-1.79 (m, 1H), 0.96 (s, 9H), two protons not detected (NH<sub>2</sub>). <sup>13</sup>C NMR (125 MHz, DMSO-d<sub>6</sub>) δ = 172.7, 169.8, 169.4, 152.0, 148.2, 139.7, 131.6, 130.2, 129.2, 127.9, 70.8, 70.2, 70.1, 70.1, 70.0, 69.5, 59.0, 56.3, 56.1, 42.3, 37.4, 35.7, 26.6, 16.4, two carbons not detected. HRMS (*m/z*): [M+H]<sup>+</sup> calculated for C<sub>30</sub>H<sub>45</sub>N<sub>5</sub>O<sub>7</sub>S, 619.30397; found, 619.30308. HPLC-MS <sup>t</sup>R = 1.01 min.

**(2S,4S)-4-hydroxy-1-[(2S)-2-(2-{2-[2-(2-{[3-methoxy-4-({4-[(3-oxo-2,3-dihydro-1H-inden-4-yl)oxy]-5-(trifluoromethyl)pyrimidin-2-yl}amino)phenyl]formamido}ethoxy)ethoxy]ethoxy}acetamido)-3,3-dimethylbutanoyl]-N-{[4-(4-methyl-1,3-thiazol-5-yl)phenyl]methyl}pyrrolidine-2-carboxamide (11, BI-4206).** In a glass vial, 3-methoxy-4-({4-

1  
2  
3 [(3-oxo-2,3-dihydro-1*H*-inden-4-yl)oxy]-5-(trifluoromethyl)pyrimidin-2-yl} amino)benzoic acid  
4  
5 (2, 116 mg, 1 eq) was dissolved in DMF (2 mL). DIPEA (100  $\mu$ L, 3 eq) and HATU (106 mg, 1.2  
6  
7 eq) were added. The reaction mixture was stirred at rt for 5 min, then (2*S*,4*S*)-1-[(2*S*)-2-(2-{2-[2-  
8  
9 (2-aminoethoxy)ethoxy]ethoxy}acetamido)-3,3-dimethylbutanoyl]-4-hydroxy-*N*-{[4-(4-methyl-  
10  
11 1,3-thiazol-5-yl)phenyl]methyl}pyrrolidine-2-carboxamide (**10b**, 144 mg, 1 eq) was added. The  
12  
13 mixture was stirred at rt for 16 h. The reaction mixture was diluted with MeCN and H<sub>2</sub>O and  
14  
15 filtered through a syringe filter prior to purification *via* RP-HPLC under basic conditions using  
16  
17 MeCN/H<sub>2</sub>O as eluents in a gradient from 30:70 to 98:2 over 8 min (column: YMC Actus-Triart  
18  
19 Prep C18, 5  $\mu$ m, 30x50 mm; flow: 50 mL/min). Product containing fractions were freeze dried to  
20  
21 give (2*S*,4*S*)-4-hydroxy-1-[(2*S*)-2-(2-{2-[2-(2-{[3-methoxy-4-(4-[(3-oxo-2,3-dihydro-1*H*-inden-  
22  
23 4-yl)oxy]-5-(trifluoromethyl)pyrimidin-2-yl} amino)phenyl]formamido} ethoxy)  
24  
25 ethoxy]ethoxy}acetamido)-3,3-dimethylbutanoyl]-*N*-{[4-(4-methyl-1,3-thiazol-5-  
26  
27 yl)phenyl]methyl}pyrrolidine-2-carboxamide (**11**, (**BI-4206**), 169 mg, 69% yield) as off-white  
28  
29 lyophilizate. <sup>1</sup>H NMR (500 MHz, DMSO-*d*<sub>6</sub>)  $\delta$  = 8.97 (s, 1H), 8.81 (br s, 1H), 8.70 (s, 1H), 8.66  
30  
31 (t, *J*=5.99 Hz, 1H), 8.45 (t, *J*=5.52 Hz, 1H), 7.77 (dd, *J*=7.57, 7.88 Hz, 1H), 7.56 (d, *J*=7.57 Hz,  
32  
33 1H), 7.35-7.45 (m, 6H), 7.21 (d, *J*=7.88 Hz, 1H), 7.25 (br s, 1H), 7.11 (br s, 1H), 5.45 (br d,  
34  
35 *J*=6.62 Hz, 1H), 4.51 (d, *J*=9.14 Hz, 1H), 4.17-4.45 (m, 4H), 3.94 (s, 2H), 3.84-3.91 (m, 1H),  
36  
37 3.77 (s, 3H), 3.36-3.62 (m, 15H), 3.07-3.15 (m, 2H), 2.43 (s, 3H), 2.29-2.36 (m, 1H), 1.69-1.79  
38  
39 (m, 1H), 0.95 (s, 9H). <sup>13</sup>C NMR (125 MHz, DMSO-*d*<sub>6</sub>)  $\delta$  = 203.4, 172.7, 169.8, 169.4, 166.4,  
40  
41 166.0, 161.1, 158.3, 157.8, 151.9, 150.0, 148.2, 147.9, 139.6, 136.9, 131.6, 130.4, 130.2, 130.0,  
42  
43 129.2, 128.9, 127.9, 125.5, 121.0, 124.0, 119.5, 110.2, 101.3, 101.1, 70.9, 70.2, 70.1, 70.1, 70.0,  
44  
45 69.5, 69.5, 59.0, 56.3, 56.1, 42.3, 37.4, 36.8, 35.6, 26.6, 25.8, 16.4, two carbons not detected.  
46  
47  
48  
49  
50  
51  
52  
53  
54  
55  
56  
57  
58  
59  
60

1  
2  
3 HRMS ( $m/z$ ):  $[M+H]^+$  calculated for  $C_{52}H_{59}F_3N_8O_{11}S$ , 1060.39761; found, 1060.39665. HPLC-  
4  
5 MS  $t_R$  = 1.71 min.  
6  
7

### 8 **Protein expression and purification.**

9  
10 Human PTK2 (residues 411–689, UniProt accession number Q05397) with an N-terminal TEV  
11 cleavage site was cloned into pDEST20 vector (Invitrogen). Expression in this vector results in a  
12 fusion protein with a cleavable GST tag. Viral stocks were generated in the Bac-to-Bac system  
13 (Invitrogen) and used to infect *Trichoplusia ni* (Hi5) cells (Invitrogen). Recombinant protein was  
14 isolated from cell extracts by affinity chromatography over glutathione sepharose (GE  
15 Healthcare) in batch mode. The GST-tag was removed by incubation with Ac-TEV protease  
16 (ThermoFisher) on the resin, overnight at 4 °C. Cleaved protein was recovered, concentrated  
17 (biomax 10, Merck) and finally purified by size exclusion chromatography on HiLoad Superdex  
18 S75 (GE Healthcare). The protein was concentrated (biomax 10, Merck) to 5 mg/ml and stored  
19 in 20 mM HEPES, 250 mM NaCl, 1 mM DTT, 1 mM EDTA, pH 6.7 at -80 °C.  
20  
21  
22  
23  
24  
25  
26  
27  
28  
29  
30  
31  
32  
33

### 34 **Crystallization of the PTK2 kinasedomain BI 4464 binary complex.**

35  
36 Protein crystallization was done using the sitting drop method by incubating the protein with  
37 1 mM BI 4464 (as 50 mM stock solution) and mixing 0.2  $\mu$ L of PTK2 (4.5 mg/mL in 25 mM  
38 HEPES pH 6.7, 250 mM NaCl, 1 mM DTT, 1 mM EDTA) with 0.2  $\mu$ L of reservoir solution  
39 (7 % PEG 1500, 100 mM SPG buffer pH 6.0) at 4 °C. Crystals grew as thin plates within a few  
40 days to a final size of 150-200  $\mu$ m). Crystals were transferred to a cryo buffer (reservoir solution  
41 with 15 % ethylene glycol) and frozen in liquid nitrogen. Data were collected at the SLS beam  
42 line X06DA (Swiss Light Source, Paul Scherrer Institute) at a wavelength of 0.91 Å using the  
43 PILATUS 2M detector. The crystals belonged to space group  $P2_12_12$  with 1 monomer per  
44 asymmetric unit. Images were processed with XDS<sup>48</sup>. The structures were solved by molecular  
45  
46  
47  
48  
49  
50  
51  
52  
53  
54  
55  
56  
57  
58  
59  
60

1  
2  
3 replacement using the PDB: 2ETM as a search model. Subsequent model building and  
4  
5 refinement was done using standard protocols using CCP4<sup>49</sup>, COOT<sup>50</sup> and autoBUSTER<sup>51</sup>. Unit  
6  
7 cell parameters were  $a = 48.05 \text{ \AA}$ ,  $b = 77.09 \text{ \AA}$ ,  $c = 82.71 \text{ \AA}$  and  $\alpha, \beta, \gamma = 90^\circ$  data and the  
8  
9 structure was refined to R and  $R_{\text{free}}$  values of 18.3 % and 22.2 %, respectively, with 98.1 % of the  
10  
11 residues in Ramachandran favored regions as validated with Molprobit<sup>52</sup>. Statistics for data  
12  
13 collection and refinement can be found in supplemental table 2. The coordinates and structure  
14  
15 factors of the structures have been deposited at the Protein Data Bank with the accession code  
16  
17 6I8Z. The authors will release the atomic coordinates and experimental data upon article  
18  
19 publication  
20  
21  
22  
23

#### 24 **Cell culture.**

25  
26  
27 Cell lines were obtained through ATCC or JCRB, verified for identity by satellite repeat  
28  
29 analysis, tested for mycoplasma contamination at regular intervals and cultured in the specified  
30  
31 media in a humidified cell incubator at 37 °C and 5 % CO<sub>2</sub>. DMEM was obtained from Lonza  
32  
33 (product code BE12-604F), EMEM from ATCC (product code 30-2003), IMDM from Thermo  
34  
35 Fisher (product code 12440053), RPMI-1640 from Thermo Fisher (product code A1049101).  
36  
37 The following cell lines (product codes and culture media in parentheses) were used for the  
38  
39 described experiments: SNU-387 (CRL-2237, RPMI-1640 plus 10 % heat inactivated FCS),  
40  
41 HUH-1 (JCRB0199, DMEM plus 10 % FCS), Hep3B2.1-7 (HB-8064, EMEM plus 10 % FCS),  
42  
43 HepG2 (HB-8065, EMEM plus 10 % FCS plus Glutamax), SK-Hep-1 HLF (JCRB0404 DMEM  
44  
45 plus 10 % FCS), SNU-398 (CRL-2233, RPMI1640 plus 10 % FCS), HUCCT1 (JCRB0425,  
46  
47 RPMI-1640 plus 10 % FCS), HLE (JCRB0405, DMEM plus 10 % FCS), HuH-7 (JCRB0403  
48  
49 DMEM plus 10 % FCS), SNU-423 (CRL-2238, RPMI-1640 plus 10 % FCS), A549 (CCL-185,  
50  
51  
52  
53  
54  
55  
56  
57  
58  
59  
60

1  
2  
3 F-12K plus 10 % heat inactivated FCS), HSC-3 (JCRB0623, EMEM plus 10 % FCS), C32  
4  
5 (CRL-1585, EMEM plus 10 % FCS), CFPAC-1 (CRL-1918, IMDM plus 10 % FCS).  
6  
7

### 8 **Protein degradation assays.**

9  
10 To quantify the effects of compounds on PTK2 protein levels, cells were seeded at a density of  
11  
12 125.000 cells in 0.75 mL of culture medium 24-well plates and allowed to attach for 6-8 hours.  
13  
14 Subsequently, compounds were added to the cells at logarithmic dose series using the HP Digital  
15  
16 Dispenser D300 (Tecan), normalizing for added DMSO. After compound addition, cells were  
17  
18 incubated for 18 h or the specified time intervals at 37 °C. Cells were washed with cold PBS and  
19  
20 lysed by immediate freezing in 100 µL RIPA buffer (Sigma product code R0278) supplemented  
21  
22 with 1:100 HALT Phosphatase-Protease Inhibitors (Thermo product code 1861281) at -80 °C.  
23  
24 After thawing, samples were transferred into V-bottom 96-well plates, cellular debris was  
25  
26 sedimented at 4000 rpm (Eppendorf centrifuge 5810R, rotor A-4-81). 90 µL of the supernatant  
27  
28 were transferred into a new 96-well plate and analyzed using a Wes capillary electrophoresis  
29  
30 instrument (Proteinsimple) using PTK2 antibody (Cell Signaling product code 13009) at a  
31  
32 dilution of 1:50 or PDE6D antibody (Abcam product code ab5665) at a dilution of 1:25 and  
33  
34 GAPDH antibody (Abcam product code ab9485) at a dilution of 1:2000 for normalization.  
35  
36  
37  
38  
39  
40

### 41 **Proliferation assays.**

42  
43 *Standard proliferation assay.* To test the effect of PTK2 PROTACs on proliferation, cells were  
44  
45 seeded at 1000 cells per well (2500 cells per well for suspension cell lines) in 100 µL growth  
46  
47 medium in a white bottom opaque 96-well plate and allowed to grow over night. To obtain  
48  
49 starting densities, a set of cells seeded in parallel were lysed and measured using 100 µL  
50  
51 CellTiter-Glo luminescent cell viability reagent (Promega product code G7570) per well as per  
52  
53 manufacturer's recommendation. Compounds were added to the cells at logarithmic dose series  
54  
55  
56  
57  
58  
59  
60

1  
2  
3 using the HP Digital Dispenser D300 (Tecan), normalizing for added DMSO. Doxorubicin  
4 (Sigma product code D1515) was used as a positive control. Upon compound addition, cells  
5 (Sigma product code D1515) was used as a positive control. Upon compound addition, cells  
6 were incubated for six days and viability measured CellTiterGlow reagent as described above.  
7  
8 Results are stated as mean and standard deviation of triplicate experiments.  
9  
10  
11

12  
13 *Anchorage independent growth assays.* Cells were seeded in 0.3 % agarose (Gibco product  
14 code 18300-012) containing cultivation medium (60  $\mu$ L) on top of a bottom layer composed of  
15 1.2 % agarose in cultivation medium (90  $\mu$ L) in 96-well plates. Upon solidification of the cell  
16 layer, the culture was overlaid with 50  $\mu$ L cultivation medium and compounds were added as  
17 indicated above. Cultures were allowed to grow for 7-14 days, stained with alamar blue reagent  
18 (Thermo Fisher product code DAL1025) and measured using a fluorescence plate reader (Wallac  
19 Victor 1420, 544 nm excitation, 590 nm emission, 0.2 s).  
20  
21  
22  
23  
24  
25  
26  
27  
28  
29

30 *Long-term proliferation assay.* Cells were inoculated at a density of 250,000 cells in 1.5 mL  
31 culture medium in 6 well plates. Compounds or DMSO were added, and every 3 to 4 days cells  
32 were split to 250,000 cells. Upon splitting, fresh compound was added to keep the concentration  
33 constant. Split rates were recorded and multiplied to derive cumulative cell counts which were  
34 converted into population doublings (n) using the formula  $n = (\log(N_x) - \log(N_0)) / \log 2$  with  $N_x$   
35 indicating the cumulative cell count at time-point x and  $N_0$  the initial seeding cell count.  
36  
37  
38  
39  
40  
41  
42  
43  
44

#### 45 **MS proteomics.**

46  
47 *Sample preparation.* A549 cells were seeded at  $5 \times 10^6$  cells/mL in a 10 cm plate 18 h before  
48 treatment. Cells were treated with 0.1% DMSO as vehicle control, 3  $\mu$ M of either active  
49 PROTAC **6** or **8**, and 3  $\mu$ M of *cis*VHL **11** as negative control. Cells were incubated at 37 °C and  
50 5 % CO<sub>2</sub> for 18 h before harvesting. Cells were washed twice with DPBS (Gibco) and lysed with  
51  
52  
53  
54  
55  
56  
57  
58  
59  
60

1  
2  
3 0.5 mL of 100 mM Tris pH 8.0, 4 % (w/v) SDS, supplemented with cOmplete™ Mini EDTA-  
4 free Protease Inhibitor Cocktail (Roche). Lysates were sonicated (2 x 10 s) and centrifuged at  
5  
6 14,000 rpm for 20 min at 4 °C. The supernatant fraction of the cell extract was collected and  
7  
8 protein concentration was quantified by BCA assay (Thermo Fisher Scientific). Further sample  
9  
10 processing, digestion, desalting, TMT 10-plex isobaric labelling were performed as previously  
11  
12 described.<sup>5</sup> After labelling, the peptides from the 9 samples were pooled together in equal  
13  
14 proportion. The pooled sample was fractionated using high pH reverse-phase chromatography on  
15  
16 an XBridge peptide BEH column (130 Å, 3.5 µm, 2.1 × 150 mm, Waters) on an Ultimate 3000  
17  
18 HPLC system (Thermo Scientific/Dionex). A mixture of Buffer A (10 mM ammonium formate  
19  
20 in water, pH 9) and B (10 mM ammonium formate in 90 % CH<sub>3</sub>CN, pH 9) was used over a  
21  
22 linear gradient of 5 % to 60 % buffer B over 60 min at a flow rate of 200 µL/min. The peptides  
23  
24 eluted from the column were collected in 80 fractions before concatenation into 20 fractions  
25  
26 based on the UV signal of each fraction. All the fractions were dried in a Genevac EZ-2  
27  
28 concentrator and resuspended in 1 % formic acid for MS analysis.  
29  
30  
31  
32  
33  
34

35 *nLC-MS/MS analysis.* The fractions were analyzed sequentially on a Q Exactive HF-X Hybrid  
36  
37 Quadrupole-Orbitrap Mass Spectrometer (Thermo Scientific) coupled to an UltiMate 3000  
38  
39 RSLCnano UHPLC system (Thermo Scientific) and EasySpray column (75 µm × 50 cm,  
40  
41 PepMap RSLC C18 column, 2 µm, 100 Å, Thermo Scientific). A mix of buffer A (0.1 % formic  
42  
43 acid in H<sub>2</sub>O) and B (0.08 % formic acid in 80 % CH<sub>3</sub>CN) was used over a linear gradient from  
44  
45 5 % to 35 % buffer B over 125 min using a flow rate of 300 nL/min. The column temperature  
46  
47 was set at 50 °C. The mass Spectrometer was operated in data dependent mode with a single MS  
48  
49 survey scan from 335-1,600 *m/z* followed by 15 sequential *m/z* dependent MS<sub>2</sub> scans. The 15  
50  
51 most intense precursor ions were sequentially fragmented by higher energy collision dissociation  
52  
53  
54  
55  
56  
57  
58  
59  
60



1  
2  
3 (HCD). The MS1 isolation window was set to 0.7  $m/z$  and the resolution set at 120,000. MS2  
4  
5 resolution was set at 45,000. The AGC targets for MS1 and MS2 were set at  $3e^6$  ions and  $1e^5$   
6  
7 ions, respectively. The normalized collision energy was set at 32 %. The maximum ion injection  
8  
9 times for MS1 and MS2 were set at 50 ms and 200 ms, respectively.  
10  
11

12 *Peptide and protein identification and quantification.* The raw MS data files for all 20 fractions  
13  
14 were merged and searched against the Uniprot-sprot-Human-Canonical database by Maxquant  
15  
16 software 1.6.0.16 for protein identification and TMT reporter ion quantitation. The  
17  
18 identifications were based on the following criteria: enzyme used Trypsin/P; maximum number  
19  
20 of missed cleavages equal to two; precursor mass tolerance equal to 10 p.p.m.; fragment mass  
21  
22 tolerance equal to 20 p.p.m.; variable modifications: Oxidation (M), Acetyl (N-term),  
23  
24 Deamidation (NQ), Gln  $\rightarrow$  pyro-Glu (Q N-term); fixed modifications: Carbamidomethyl (C).  
25  
26 The data was filtered by applying a 1 % false discovery rate followed by exclusion of proteins  
27  
28 with less than two unique peptides. Quantified proteins were filtered if the absolute fold-change  
29  
30 difference between the three DMSO replicates was  $\geq 1.5$ .  
31  
32  
33  
34  
35  
36

## 37 **AUTHOR INFORMATION**

### 38 **Corresponding Author**

39  
40  
41  
42 \* To whom correspondence should be addressed: Peter Ettmayer, E-mail:

43  
44 peter.ettmayer@boehringer-ingenelheim.com  
45  
46

### 47 **Present Addresses**

48  
49  
50 † Present address (C.M.): Boehringer Ingelheim RCV GmbH & Co KG, 1221, Vienna, Austria.  
51  
52  
53  
54  
55  
56  
57  
58  
59  
60

### Author Contributions

The manuscript was written through contributions of all authors. All authors have given approval to the final version of the manuscript.

### FUNDING SOURCES

### NOTES

While this manuscript was in advanced preparation selective VHL based PTK2 PROTACs were published by P. M. Cromm et al. J. Am. Chem. Soc., DOI: 10.1021/jacs.8b08008 as a manuscript just accepted, describing a VHL-based degrader (PROTAC-3) with chemical structure different from BI-0319.

### ACKNOWLEDGMENT

We would like to thank Will Farnaby for coordination of the proteomics study, Moriz Mayer for coordinating the analytics, Gerlinde Flotzinger for PTK2 protein expression and purification, and Gabriele Glenndining and Susanne Mayer for their excellent logistics work for the collaboration between Boehringer Ingelheim and University of Dundee.

### ABBREVIATIONS

NH<sub>4</sub>OAc, ammonium acetate; BET, bromodomain and extra-terminal; BRD2/3/4/7/9, bromodomain-containing protein 2/3/4/7/9; CRBN, cereblon; DLBCL, Diffuse Large B Cell Lymphoma; HCl, Hydrochloric acid; DIPEA, N,N-Diisopropylethylamine; EtOH, ethanol; EtOAc, ethyl acetate; H<sub>2</sub>O, water; HATU, 1-[Bis(dimethylamino)methylene]-1H-1,2,3-triazolo[4,5-b]pyridinium 3-oxid hexafluorophosphate; HOAt, 1-Hydroxy-7-azabenzotriazole

1  
2  
3 solution; MgSO<sub>4</sub>, magnesium sulfate; MsCl, methanesulfonyl chloride; PROTAC, proteolysis-  
4 targeting chimera; NaHCO<sub>3</sub>, sodium bicarbonate; NaHDMS, Sodium bis(trimethylsilyl)amide;  
5  
6 NaH, sodium hydride; NaOH, sodium hydroxide; NaIO<sub>4</sub>, sodium periodate; NaBH(OAc)<sub>3</sub>,  
7  
8 sodium triacetoxyborohydride; OsO<sub>4</sub>, osmium tetroxide; TEMPO, 2,2,6,6-Tetramethyl-1-  
9  
10 piperidinyloxy; VHL; von Hippel-Lindau.  
11  
12  
13

## 14 15 **ASSOCIATED CONTENT**

### 16 17 **Supporting Information**

18  
19 The supporting information is available free of charge on the ACS Publication website at  
20  
21 DOI:....  
22  
23

24  
25  
26  
27 Additional PTK2 degradation data for BI-0319 and BI-3663 in HCC cell lines (SNU387, HUH-  
28  
29 1, Hep3B2.1-7, HepG2, SK-Hep1, HLF, SNU-398, HUCCT1, HLE, HuH7, SNU-423); Alamar  
30  
31 Blue cell viability assays in above HCC cell lines with BI-3663, BI-0319, BI-4464 and  
32  
33 doxorubicine (positive control); Long-term proliferation assays in HSC-3, C32, CFPAC-1 and  
34  
35 A549 with 3 μM of of BI-3663 or BI-0319; CRISPR validation of PTK2 dependency, Solubility,  
36  
37 plasma protein binding and Caco2 permeability assay data for PROTACs BI-0319 and BI-3663;  
38  
39 X-ray Data collection and refinement statistics; Supplementary chemistry information: MS  
40  
41 parameters, HPLC chromatograms and NMR spectrum of BI-3663; Supplemental methods:  
42  
43 solubility, PPB, CACO2 permeability, stability measurement, CRISPR depletion of PTK2 .  
44  
45  
46  
47

48  
49 Molecular formula strings (CSV)

50  
51  
52 Proteomics raw data (XLSX)

### 53 54 55 **Accession Codes**

1  
2  
3 Atomic coordinates and structure factors for PTK2:BI-4464 have been deposited to the Protein  
4 Data Bank (PDB) under accession number 6I8Z. Authors will release the atomic coordinates and  
5  
6 experimental data upon article publication  
7  
8  
9  
10

## 11 REFERENCES

- 12  
13  
14 1. Golubovskaya, V. M. Targeting FAK in human cancer: from finding to first clinical trials.  
15  
16 *Front Biosci (Landmark Ed)* **2014**, 19, 687-706.  
17
- 18  
19 2. Sulzmaier, F. J.; Jean, C.; Schlaepfer, D. D. FAK in cancer: mechanistic findings and  
20  
21 clinical applications. *Nat Rev Cancer* **2014**, 14, 598-610.  
22
- 23  
24 3. Lark, A. L.; Livasy, C. A.; Calvo, B.; Caskey, L.; Moore, D. T.; Yang, X.; Cance, W. G.  
25  
26 Overexpression of focal adhesion kinase in primary colorectal carcinomas and colorectal liver  
27  
28 metastases: immunohistochemistry and real-time PCR analyses. *Clin Cancer Res* **2003**, 9, 215-  
29  
30 222.  
31
- 32  
33 4. Judson, P. L.; He, X.; Cance, W. G.; Van Le, L. Overexpression of focal adhesion kinase,  
34  
35 a protein tyrosine kinase, in ovarian carcinoma. *Cancer* **1999**, 86, 1551-1556.  
36
- 37  
38 5. Miyazaki, T.; Kato, H.; Nakajima, M.; Sohda, M.; Fukai, Y.; Masuda, N.; Manda, R.;  
39  
40 Fukuchi, M.; Tsukada, K.; Kuwano, H. FAK overexpression is correlated with tumour  
41  
42 invasiveness and lymph node metastasis in oesophageal squamous cell carcinoma. *Br J Cancer*  
43  
44 **2003**, 89, 140-145.  
45
- 46  
47 6. Itoh, S.; Maeda, T.; Shimada, M.; Aishima, S.; Shirabe, K.; Tanaka, S.; Maehara, Y. Role  
48  
49 of expression of focal adhesion kinase in progression of hepatocellular carcinoma. *Clin Cancer*  
50  
51 *Res* **2004**, 10, 2812-2817.  
52
- 53  
54 7. Sood, A. K.; Armaiz-Pena, G. N.; Halder, J.; Nick, A. M.; Stone, R. L.; Hu, W.; Carroll,  
55  
56 A. R.; Spannuth, W. A.; Deavers, M. T.; Allen, J. K.; Han, L. Y.; Kamat, A. A.; Shahzad, M. M.;  
57  
58  
59

1  
2  
3 McIntyre, B. W.; Diaz-Montero, C. M.; Jennings, N. B.; Lin, Y. G.; Merritt, W. M.; DeGeest, K.;  
4  
5 Vivas-Mejia, P. E.; Lopez-Berestein, G.; Schaller, M. D.; Cole, S. W.; Lutgendorf, S. K.

6  
7 Adrenergic modulation of focal adhesion kinase protects human ovarian cancer cells from  
8  
9 anoikis. *J Clin Invest* **2010**, 120, 1515-1523.

10  
11  
12 8. Ward, K. K.; Tancioni, I.; Lawson, C.; Miller, N. L.; Jean, C.; Chen, X. L.; Uryu, S.; Kim,  
13  
14 J.; Tarin, D.; Stupack, D. G.; Plaxe, S. C.; Schlaepfer, D. D. Inhibition of focal adhesion kinase  
15  
16 (FAK) activity prevents anchorage-independent ovarian carcinoma cell growth and tumor  
17  
18 progression. *Clin Exp Metastasis* **2013**, 30, 579-594.

19  
20  
21 9. Balogh, J.; Victor, D., 3rd; Asham, E. H.; Burroughs, S. G.; Boktour, M.; Saharia, A.; Li,  
22  
23 X.; Ghobrial, R. M.; Monsour, H. P., Jr. Hepatocellular carcinoma: a review. *J Hepatocell*  
24  
25 *Carcinoma* **2016**, 3, 41-53.

26  
27  
28 10. El-Serag, H. B. Hepatocellular carcinoma. *N Engl J Med* **2011**, 365, 1118-1127.

29  
30  
31 11. Llovet, J. M.; Schwartz, M.; Mazzaferro, V. Resection and liver transplantation for  
32  
33 hepatocellular carcinoma. *Semin Liver Dis* **2005**, 25, 181-200.

34  
35  
36 12. Xu, Q.; Kobayashi, S.; Ye, X.; Meng, X. Comparison of hepatic resection and  
37  
38 radiofrequency ablation for small hepatocellular carcinoma: a meta-analysis of 16,103 patients.  
39  
40 *Sci Rep* **2014**, 4, 7252.

41  
42  
43 13. Li, W. X.; Chen, L. P.; Sun, M. Y.; Li, J. T.; Liu, H. Z.; Zhu, W. 3'3-Diindolylmethane  
44  
45 inhibits migration, invasion and metastasis of hepatocellular carcinoma by suppressing FAK  
46  
47 signaling. *Oncotarget* **2015**, 6, 23776-23792.

48  
49  
50 14. Gnani, D.; Romito, I.; Artuso, S.; Chierici, M.; De Stefanis, C.; Panera, N.; Crudele, A.;  
51  
52 Ceccarelli, S.; Carcarino, E.; D'Oria, V.; Porru, M.; Giorda, E.; Ferrari, K.; Miele, L.; Villa, E.;  
53  
54 Balsano, C.; Pasini, D.; Furlanello, C.; Locatelli, F.; Nobili, V.; Rota, R.; Leonetti, C.; Alisi, A.

1  
2  
3 Focal adhesion kinase depletion reduces human hepatocellular carcinoma growth by repressing  
4 enhancer of zeste homolog 2. *Cell Death Differ* **2017**, *24*, 889-902.

5  
6  
7  
8 15. Hirt, U. A.; Waizenegger, I. C.; Schweifer, N.; Haslinger, C.; Gerlach, D.; Braunger, J.;  
9 Weyer-Czernilofsky, U.; Stadtmuller, H.; Sapountzis, I.; Bader, G.; Zoephel, A.; Bister, B.;  
10 Baum, A.; Quant, J.; Kraut, N.; Garin-Chesa, P.; Adolf, G. R. Efficacy of the highly selective  
11 focal adhesion kinase inhibitor BI 853520 in adenocarcinoma xenograft models is linked to a  
12 mesenchymal tumor phenotype. *Oncogenesis* **2018**, *7*, 21.

13  
14  
15  
16  
17  
18  
19 16. Tiede, S.; Meyer-Schaller, N.; Kalathur, R. K. R.; Ivanek, R.; Fagiani, E.; Schmassmann,  
20 P.; Stillhard, P.; Hafliger, S.; Kraut, N.; Schweifer, N.; Waizenegger, I. C.; Bill, R.; Christofori,  
21 G. The FAK inhibitor BI 853520 exerts anti-tumor effects in breast cancer. *Oncogenesis* **2018**, *7*,  
22 73.

23  
24  
25  
26  
27  
28 17. Tanjoni, I.; Walsh, C.; Uryu, S.; Tomar, A.; Nam, J. O.; Mielgo, A.; Lim, S. T.; Liang, C.;  
29 Koenig, M.; Sun, C.; Patel, N.; Kwok, C.; McMahon, G.; Stupack, D. G.; Schlaepfer, D. D.  
30 PND-1186 FAK inhibitor selectively promotes tumor cell apoptosis in three-dimensional  
31 environments. *Cancer Biol Ther* **2010**, *9*, 764-777.

32  
33  
34  
35  
36  
37 18. Cance, W. G.; Golubovskaya, V. M. Focal adhesion kinase versus p53: apoptosis or  
38 survival? *Sci Signal* **2008**, *1*, pe22.

39  
40  
41  
42 19. Sakamoto, K. M.; Kim, K. B.; Kumagai, A.; Mercurio, F.; Crews, C. M.; Deshaies, R. J.  
43  
44  
45  
46  
47  
48  
49  
50  
51  
52  
53  
54  
55  
56  
57  
58  
59  
60  
61  
62  
63  
64  
65  
66  
67  
68  
69  
70  
71  
72  
73  
74  
75  
76  
77  
78  
79  
80  
81  
82  
83  
84  
85  
86  
87  
88  
89  
90  
91  
92  
93  
94  
95  
96  
97  
98  
99  
100  
101  
102  
103  
104  
105  
106  
107  
108  
109  
110  
111  
112  
113  
114  
115  
116  
117  
118  
119  
120  
121  
122  
123  
124  
125  
126  
127  
128  
129  
130  
131  
132  
133  
134  
135  
136  
137  
138  
139  
140  
141  
142  
143  
144  
145  
146  
147  
148  
149  
150  
151  
152  
153  
154  
155  
156  
157  
158  
159  
160  
161  
162  
163  
164  
165  
166  
167  
168  
169  
170  
171  
172  
173  
174  
175  
176  
177  
178  
179  
180  
181  
182  
183  
184  
185  
186  
187  
188  
189  
190  
191  
192  
193  
194  
195  
196  
197  
198  
199  
200  
201  
202  
203  
204  
205  
206  
207  
208  
209  
210  
211  
212  
213  
214  
215  
216  
217  
218  
219  
220  
221  
222  
223  
224  
225  
226  
227  
228  
229  
230  
231  
232  
233  
234  
235  
236  
237  
238  
239  
240  
241  
242  
243  
244  
245  
246  
247  
248  
249  
250  
251  
252  
253  
254  
255  
256  
257  
258  
259  
260  
261  
262  
263  
264  
265  
266  
267  
268  
269  
270  
271  
272  
273  
274  
275  
276  
277  
278  
279  
280  
281  
282  
283  
284  
285  
286  
287  
288  
289  
290  
291  
292  
293  
294  
295  
296  
297  
298  
299  
300  
301  
302  
303  
304  
305  
306  
307  
308  
309  
310  
311  
312  
313  
314  
315  
316  
317  
318  
319  
320  
321  
322  
323  
324  
325  
326  
327  
328  
329  
330  
331  
332  
333  
334  
335  
336  
337  
338  
339  
340  
341  
342  
343  
344  
345  
346  
347  
348  
349  
350  
351  
352  
353  
354  
355  
356  
357  
358  
359  
360  
361  
362  
363  
364  
365  
366  
367  
368  
369  
370  
371  
372  
373  
374  
375  
376  
377  
378  
379  
380  
381  
382  
383  
384  
385  
386  
387  
388  
389  
390  
391  
392  
393  
394  
395  
396  
397  
398  
399  
400  
401  
402  
403  
404  
405  
406  
407  
408  
409  
410  
411  
412  
413  
414  
415  
416  
417  
418  
419  
420  
421  
422  
423  
424  
425  
426  
427  
428  
429  
430  
431  
432  
433  
434  
435  
436  
437  
438  
439  
440  
441  
442  
443  
444  
445  
446  
447  
448  
449  
450  
451  
452  
453  
454  
455  
456  
457  
458  
459  
460  
461  
462  
463  
464  
465  
466  
467  
468  
469  
470  
471  
472  
473  
474  
475  
476  
477  
478  
479  
480  
481  
482  
483  
484  
485  
486  
487  
488  
489  
490  
491  
492  
493  
494  
495  
496  
497  
498  
499  
500  
501  
502  
503  
504  
505  
506  
507  
508  
509  
510  
511  
512  
513  
514  
515  
516  
517  
518  
519  
520  
521  
522  
523  
524  
525  
526  
527  
528  
529  
530  
531  
532  
533  
534  
535  
536  
537  
538  
539  
540  
541  
542  
543  
544  
545  
546  
547  
548  
549  
550  
551  
552  
553  
554  
555  
556  
557  
558  
559  
560  
561  
562  
563  
564  
565  
566  
567  
568  
569  
570  
571  
572  
573  
574  
575  
576  
577  
578  
579  
580  
581  
582  
583  
584  
585  
586  
587  
588  
589  
590  
591  
592  
593  
594  
595  
596  
597  
598  
599  
600  
601  
602  
603  
604  
605  
606  
607  
608  
609  
610  
611  
612  
613  
614  
615  
616  
617  
618  
619  
620  
621  
622  
623  
624  
625  
626  
627  
628  
629  
630  
631  
632  
633  
634  
635  
636  
637  
638  
639  
640  
641  
642  
643  
644  
645  
646  
647  
648  
649  
650  
651  
652  
653  
654  
655  
656  
657  
658  
659  
660  
661  
662  
663  
664  
665  
666  
667  
668  
669  
670  
671  
672  
673  
674  
675  
676  
677  
678  
679  
680  
681  
682  
683  
684  
685  
686  
687  
688  
689  
690  
691  
692  
693  
694  
695  
696  
697  
698  
699  
700  
701  
702  
703  
704  
705  
706  
707  
708  
709  
710  
711  
712  
713  
714  
715  
716  
717  
718  
719  
720  
721  
722  
723  
724  
725  
726  
727  
728  
729  
730  
731  
732  
733  
734  
735  
736  
737  
738  
739  
740  
741  
742  
743  
744  
745  
746  
747  
748  
749  
750  
751  
752  
753  
754  
755  
756  
757  
758  
759  
760  
761  
762  
763  
764  
765  
766  
767  
768  
769  
770  
771  
772  
773  
774  
775  
776  
777  
778  
779  
780  
781  
782  
783  
784  
785  
786  
787  
788  
789  
790  
791  
792  
793  
794  
795  
796  
797  
798  
799  
800  
801  
802  
803  
804  
805  
806  
807  
808  
809  
810  
811  
812  
813  
814  
815  
816  
817  
818  
819  
820  
821  
822  
823  
824  
825  
826  
827  
828  
829  
830  
831  
832  
833  
834  
835  
836  
837  
838  
839  
840  
841  
842  
843  
844  
845  
846  
847  
848  
849  
850  
851  
852  
853  
854  
855  
856  
857  
858  
859  
860  
861  
862  
863  
864  
865  
866  
867  
868  
869  
870  
871  
872  
873  
874  
875  
876  
877  
878  
879  
880  
881  
882  
883  
884  
885  
886  
887  
888  
889  
890  
891  
892  
893  
894  
895  
896  
897  
898  
899  
900  
901  
902  
903  
904  
905  
906  
907  
908  
909  
910  
911  
912  
913  
914  
915  
916  
917  
918  
919  
920  
921  
922  
923  
924  
925  
926  
927  
928  
929  
930  
931  
932  
933  
934  
935  
936  
937  
938  
939  
940  
941  
942  
943  
944  
945  
946  
947  
948  
949  
950  
951  
952  
953  
954  
955  
956  
957  
958  
959  
960  
961  
962  
963  
964  
965  
966  
967  
968  
969  
970  
971  
972  
973  
974  
975  
976  
977  
978  
979  
980  
981  
982  
983  
984  
985  
986  
987  
988  
989  
990  
991  
992  
993  
994  
995  
996  
997  
998  
999  
1000

18. Ottis, P.; Crews, C. M. Proteolysis-targeting chimeras: induced protein degradation as a  
therapeutic strategy. *ACS Chem Biol* **2017**, *12*, 892-898.

- 1  
2  
3 21. Collins, I.; Wang, H.; Caldwell, J. J.; Chopra, R. Chemical approaches to targeted protein  
4 degradation through modulation of the ubiquitin-proteasome pathway. *Biochem J* **2017**, 474,  
5 1127-1147.  
6  
7  
8  
9  
10 22. Lai, A. C.; Crews, C. M. Induced protein degradation: an emerging drug discovery  
11 paradigm. *Nat Rev Drug Discov* **2017**, 16, 101-114.  
12  
13  
14 23. Hughes, S. J.; Ciulli, A. Molecular recognition of ternary complexes: a new dimension in  
15 the structure-guided design of chemical degraders. *Essays Biochem* **2017**, 61, 505-516.  
16  
17  
18  
19 24. Nowak, R. P.; DeAngelo, S. L.; Buckley, D.; He, Z.; Donovan, K. A.; An, J.; Safaei, N.;  
20 Jedrychowski, M. P.; Ponthier, C. M.; Ishoey, M.; Zhang, T.; Mancias, J. D.; Gray, N. S.;  
21 Bradner, J. E.; Fischer, E. S. Plasticity in binding confers selectivity in ligand-induced protein  
22 degradation. *Nat Chem Biol* **2018**, 706-714.  
23  
24  
25  
26  
27  
28 25. Gadd, M. S.; Testa, A.; Lucas, X.; Chan, K. H.; Chen, W.; Lamont, D. J.; Zengerle, M.;  
29 Ciulli, A. Structural basis of PROTAC cooperative recognition for selective protein degradation.  
30 *Nat Chem Biol* **2017**, 13, 514-521.  
31  
32  
33  
34  
35 26. Chan, K. H.; Zengerle, M.; Testa, A.; Ciulli, A. Impact of target warhead and linkage  
36 vector on inducing protein degradation: comparison of bromodomain and extra-terminal (BET)  
37 degraders derived from triazolodiazepine (JQ1) and tetrahydroquinoline (I-BET726) BET  
38 inhibitor scaffolds. *J Med Chem* **2018**, 61, 504-513.  
39  
40  
41  
42  
43  
44 27. Bondeson, D. P.; Smith, B. E.; Burslem, G. M.; Buhimschi, A. D.; Hines, J.; Jaime-  
45 Figueroa, S.; Wang, J.; Hamman, B. D.; Ishchenko, A.; Crews, C. M. Lessons in PROTAC  
46 design from selective degradation with a promiscuous warhead. *Cell Chem Biol* **2018**, 25, 78-87  
47  
48  
49  
50  
51 e5.  
52  
53  
54  
55  
56  
57  
58  
59  
60

- 1  
2  
3 28. Zengerle, M.; Chan, K. H.; Ciulli, A. Selective small molecule induced degradation of the  
4 BET bromodomain protein BRD4. *ACS Chem Biol* **2015**, 10, 1770-1777.  
5  
6  
7 29. Remillard, D.; Buckley, D. L.; Paulk, J.; Brien, G. L.; Sonnett, M.; Seo, H. S.; Dastjerdi,  
8 S.; Wuhr, M.; Dhe-Paganon, S.; Armstrong, S. A.; Bradner, J. E. Degradation of the BAF  
9 complex factor BRD9 by heterobifunctional ligands. *Angew Chem Int Ed Engl* **2017**, 56, 5738-  
10 5743.  
11  
12 30. Winter, G. E.; Buckley, D. L.; Paulk, J.; Roberts, J. M.; Souza, A.; Dhe-Paganon, S.;  
13 Bradner, J. E. Drug development: phthalimide conjugation as a strategy for in vivo target protein  
14 degradation. *Science* **2015**, 348, 1376-1381.  
15  
16 31. Lai, A. C.; Toure, M.; Hellerschmied, D.; Salami, J.; Jaime-Figueroa, S.; Ko, E.; Hines, J.;  
17 Crews, C. M. Modular PROTAC design for the degradation of oncogenic BCR-ABL. *Angew*  
18 *Chem Int Ed Engl* **2016**, 55, 807-810.  
19  
20 32. Petroski, M. D.; Deshaies, R. J. Function and regulation of cullin-RING ubiquitin ligases.  
21 *Nat Rev Mol Cell Biol* **2005**, 6, 9-20.  
22  
23 33. Zhu, Y. X.; Braggio, E.; Shi, C. X.; Bruins, L. A.; Schmidt, J. E.; Van Wier, S.; Chang, X.  
24 B.; Bjorklund, C. C.; Fonseca, R.; Bergsagel, P. L.; Orłowski, R. Z.; Stewart, A. K. Cereblon  
25 expression is required for the antimyeloma activity of lenalidomide and pomalidomide. *Blood*  
26 **2011**, 118, 4771-4779.  
27  
28 34. Powell, C. E.; Gao, Y.; Tan, L.; Donovan, K. A.; Nowak, R. P.; Loehr, A.; Bahcall, M.;  
29 Fischer, E. S.; Janne, P. A.; George, R. E.; Gray, N. S. Chemically induced degradation of  
30 anaplastic lymphoma kinase (ALK). *J Med Chem* **2018**, 61, 4249-4255.  
31  
32 35. Huang, H. T.; Dobrovolsky, D.; Paulk, J.; Yang, G.; Weisberg, E. L.; Doctor, Z. M.;  
33 Buckley, D. L.; Cho, J. H.; Ko, E.; Jang, J.; Shi, K.; Choi, H. G.; Griffin, J. D.; Li, Y.; Treon, S.  
34  
35  
36  
37  
38  
39  
40  
41  
42  
43  
44  
45  
46  
47  
48  
49  
50  
51  
52  
53  
54  
55  
56  
57  
58  
59  
60



1  
2  
3 P.; Fischer, E. S.; Bradner, J. E.; Tan, L.; Gray, N. S. A chemoproteomic approach to query the  
4 degradable kinome using a multi-kinase degrader. *Cell Chem Biol* **2018**, *25*, 88-99 e6.

5  
6  
7 36. McDonald, E. R., 3rd; de Weck, A.; Schlabach, M. R.; Billy, E.; Mavrakis, K. J.;  
8 Hoffman, G. R.; Belur, D.; Castelletti, D.; Frias, E.; Gampa, K.; Golji, J.; Kao, I.; Li, L.; Megel,  
9 P.; Perkins, T. A.; Ramadan, N.; Ruddy, D. A.; Silver, S. J.; Sovath, S.; Stump, M.; Weber, O.;  
10 Widmer, R.; Yu, J.; Yu, K.; Yue, Y.; Abramowski, D.; Ackley, E.; Barrett, R.; Berger, J.;  
11 Bernard, J. L.; Billig, R.; Brachmann, S. M.; Buxton, F.; Caothien, R.; Caushi, J. X.; Chung, F.  
12 S.; Cortes-Cros, M.; deBeaumont, R. S.; Delaunay, C.; Desplat, A.; Duong, W.; Dwoske, D. A.;  
13 Eldridge, R. S.; Farsidjani, A.; Feng, F.; Feng, J.; Flemming, D.; Forrester, W.; Galli, G. G.; Gao,  
14 Z.; Gauter, F.; Gibaja, V.; Haas, K.; Hattenberger, M.; Hood, T.; Hurov, K. E.; Jagani, Z.; Jenal,  
15 M.; Johnson, J. A.; Jones, M. D.; Kapoor, A.; Korn, J.; Liu, J.; Liu, Q.; Liu, S.; Liu, Y.; Loo, A.  
16 T.; Macchi, K. J.; Martin, T.; McAllister, G.; Meyer, A.; Molle, S.; Pagliarini, R. A.; Phadke, T.;  
17 Repko, B.; Schouwey, T.; Shanahan, F.; Shen, Q.; Stamm, C.; Stephan, C.; Stucke, V. M.; Tiedt,  
18 R.; Varadarajan, M.; Venkatesan, K.; Vitari, A. C.; Wallroth, M.; Weiler, J.; Zhang, J.; Mickanin,  
19 C.; Myer, V. E.; Porter, J. A.; Lai, A.; Bitter, H.; Lees, E.; Keen, N.; Kauffmann, A.; Stegmeier,  
20 F.; Hofmann, F.; Schmelzle, T.; Sellers, W. R. Project DRIVE: a compendium of cancer  
21 dependencies and synthetic lethal relationships uncovered by large-scale, deep RNAi screening.  
22 *Cell* **2017**, *170*, 577-592 e10.

23  
24  
25 37. Galdeano, C.; Gadd, M. S.; Soares, P.; Scaffidi, S.; Van Molle, I.; Birced, I.; Hewitt, S.;  
26 Dias, D. M.; Ciulli, A. Structure-guided design and optimization of small molecules targeting the  
27 protein-protein interaction between the von Hippel-Lindau (VHL) E3 ubiquitin ligase and the  
28 hypoxia inducible factor (HIF) alpha subunit with in vitro nanomolar affinities. *J Med Chem*  
29 **2014**, *57*, 8657-8663.

- 1  
2  
3 38. Fischer, E. S.; Bohm, K.; Lydeard, J. R.; Yang, H.; Stadler, M. B.; Cavadini, S.; Nagel, J.;  
4 Serluca, F.; Acker, V.; Lingaraju, G. M.; Tichkule, R. B.; Schebesta, M.; Forrester, W. C.;  
5  
6 Schirle, M.; Hassiepen, U.; Ottl, J.; Hild, M.; Beckwith, R. E.; Harper, J. W.; Jenkins, J. L.;  
7  
8 Thoma, N. H. Structure of the DDB1-CRBN E3 ubiquitin ligase in complex with thalidomide.  
9  
10 *Nature* **2014**, 512, 49-53.  
11  
12  
13  
14 39. Bondeson, D. P.; Mares, A.; Smith, I. E.; Ko, E.; Campos, S.; Miah, A. H.; Mulholland,  
15  
16 K. E.; Routly, N.; Buckley, D. L.; Gustafson, J. L.; Zinn, N.; Grandi, P.; Shimamura, S.;  
17  
18 Bergamini, G.; Faelth-Savitski, M.; Bantscheff, M.; Cox, C.; Gordon, D. A.; Willard, R. R.;  
19  
20 Flanagan, J. J.; Casillas, L. N.; Votta, B. J.; den Besten, W.; Famm, K.; Kruidenier, L.; Carter, P.  
21  
22 S.; Harling, J. D.; Churcher, I.; Crews, C. M. Catalytic in vivo protein knockdown by small-  
23  
24 molecule PROTACs. *Nat Chem Biol* **2015**, 11, 611-617.  
25  
26  
27  
28 40. Lu, J.; Qian, Y.; Altieri, M.; Dong, H.; Wang, J.; Raina, K.; Hines, J.; Winkler, J. D.;  
29  
30 Crew, A. P.; Coleman, K.; Crews, C. M. Hijacking the E3 ubiquitin ligase cereblon to efficiently  
31  
32 target BRD4. *Chem Biol* **2015**, 22, 755-763.  
33  
34  
35 41. Soares, P.; Gadd, M. S.; Frost, J.; Galdeano, C.; Ellis, L.; Epemolu, O.; Rocha, S.; Read,  
36  
37 K. D.; Ciulli, A. Group-based optimization of potent and cell-active inhibitors of the von Hippel-  
38  
39 Lindau (VHL) E3 ubiquitin ligase: structure-activity relationships leading to the chemical probe  
40  
41 (2S,4R)-1-((S)-2-(1-cyanocyclopropanecarboxamido)-3,3-dimethylbutanoyl)-4-hydroxy -N-(4-  
42  
43 (4-methylthiazol-5-yl)benzyl)pyrrolidine-2-carboxamide (VH298). *J Med Chem* **2018**, 61, 599-  
44  
45 618.  
46  
47  
48 42. Frost, J.; Galdeano, C.; Soares, P.; Gadd, M. S.; Grzes, K. M.; Ellis, L.; Epemolu, O.;  
49  
50 Shimamura, S.; Bantscheff, M.; Grandi, P.; Read, K. D.; Cantrell, D. A.; Rocha, S.; Ciulli, A.  
51  
52  
53  
54  
55  
56  
57  
58  
59  
60

Potent and selective chemical probe of hypoxic signalling downstream of HIF-alpha hydroxylation via VHL inhibition. *Nat Commun* **2016**, 7, 13312.

43. Soucy, T. A.; Smith, P. G.; Milhollen, M. A.; Berger, A. J.; Gavin, J. M.; Adhikari, S.; Brownell, J. E.; Burke, K. E.; Cardin, D. P.; Critchley, S.; Cullis, C. A.; Doucette, A.; Garnsey, J. J.; Gaulin, J. L.; Gershman, R. E.; Lublinsky, A. R.; McDonald, A.; Mizutani, H.; Narayanan, U.; Olhava, E. J.; Peluso, S.; Rezaei, M.; Sintchak, M. D.; Talreja, T.; Thomas, M. P.; Traore, T.; Vyskocil, S.; Weatherhead, G. S.; Yu, J.; Zhang, J.; Dick, L. R.; Claiborne, C. F.; Rolfe, M.; Bolen, J. B.; Langston, S. P. An inhibitor of NEDD8-activating enzyme as a new approach to treat cancer. *Nature* **2009**, 458, 732-736.

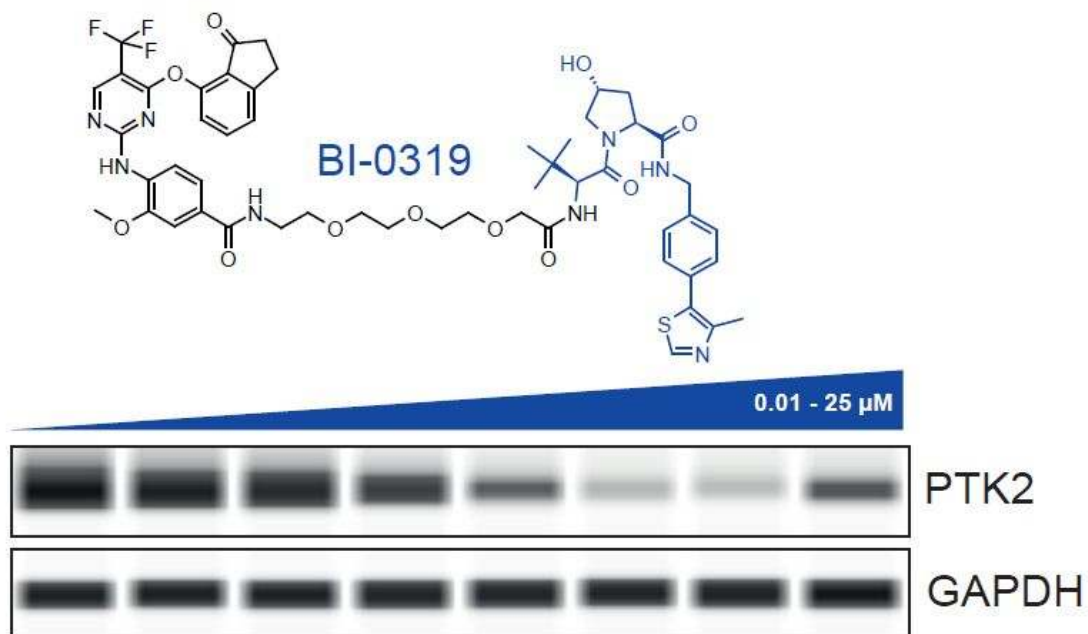
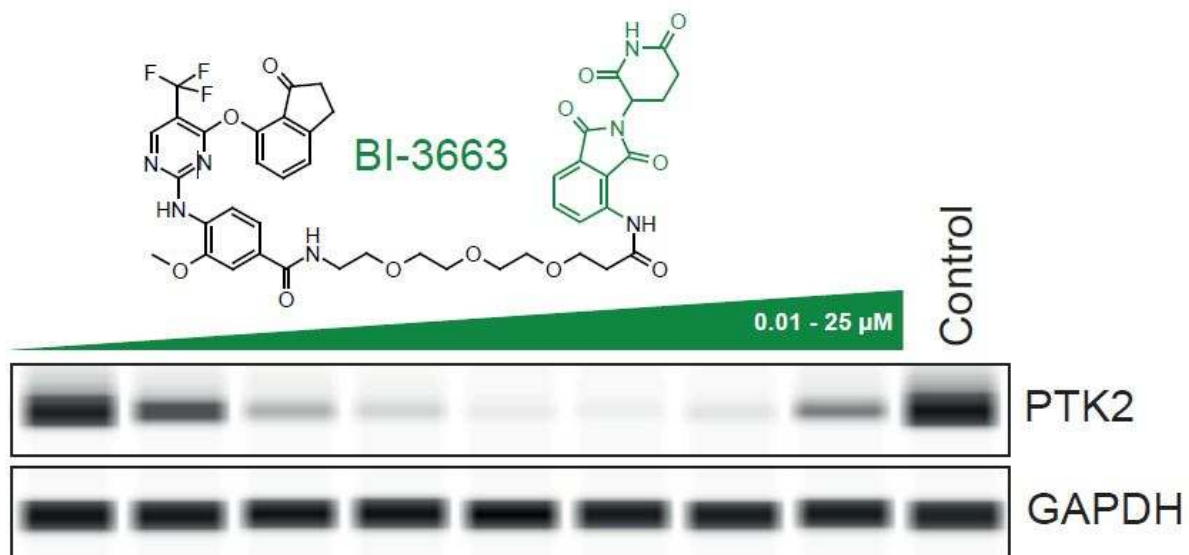
44. Saeki, T.; Ueda, K.; Tanigawara, Y.; Hori, R.; Komano, T. Human P-glycoprotein transports cyclosporin A and FK506. *J Biol Chem* **1993**, 268, 6077-6080.

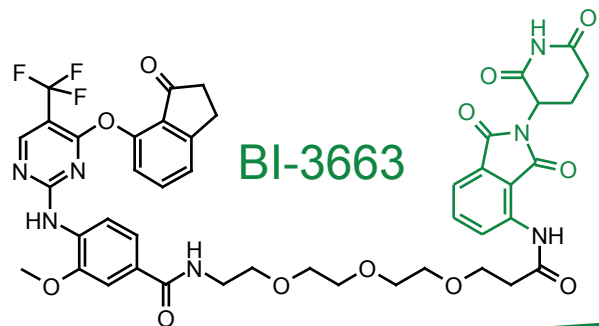
45. Chessum, N. E. A.; Sharp, S. Y.; Caldwell, J. J.; Pasqua, A. E.; Wilding, B.; Colombano, G.; Collins, I.; Ozer, B.; Richards, M.; Rowlands, M.; Stubbs, M.; Burke, R.; McAndrew, P. C.; Clarke, P. A.; Workman, P.; Cheeseman, M. D.; Jones, K. Demonstrating In-cell target engagement using a pirin protein degradation probe (CCT367766). *J Med Chem* **2018**, 61, 918-933.

46. Meyers, R. M.; Bryan, J. G.; McFarland, J. M.; Weir, B. A.; Sizemore, A. E.; Xu, H.; Dharia, N. V.; Montgomery, P. G.; Cowley, G. S.; Pantel, S.; Goodale, A.; Lee, Y.; Ali, L. D.; Jiang, G.; Lubonja, R.; Harrington, W. F.; Strickland, M.; Wu, T.; Hawes, D. C.; Zhivich, V. A.; Wyatt, M. R.; Kalani, Z.; Chang, J. J.; Okamoto, M.; Stegmaier, K.; Golub, T. R.; Boehm, J. S.; Vazquez, F.; Root, D. E.; Hahn, W. C.; Tsherniak, A. Computational correction of copy number effect improves specificity of CRISPR-Cas9 essentiality screens in cancer cells. *Nat Genet* **2017**, 49, 1779-1784.

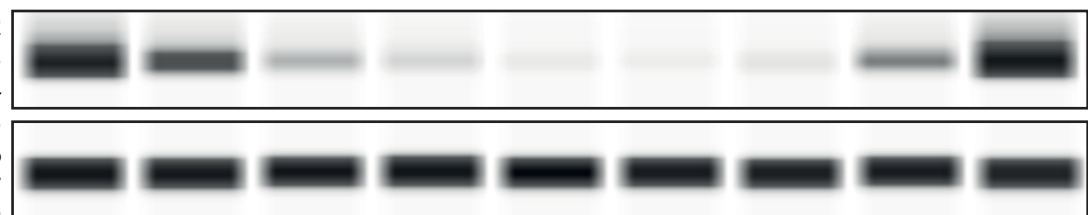
- 1  
2  
3  
4  
5  
6  
7  
8  
9  
10  
11  
12  
13  
14  
15  
16  
17  
18  
19  
20  
21  
22  
23  
24  
25  
26  
27  
28  
29  
30  
31  
32  
33  
34  
35  
36  
37  
38  
39  
40  
41  
42  
43  
44  
45  
46  
47  
48  
49  
50  
51  
52  
53  
54  
55  
56  
57  
58  
59  
60
47. Stadtmueller, H.; Sapountzis, I. Preparation of Pyrimidinamine Derivatives for Treating Diseases Characterized by Excessive or Abnormal Cell Proliferation. *Int Pat Appl* WO 2010/058032, May 27, **2010**.
48. Kabsch, W. Integration, scaling, space-group assignment and post-refinement. *Acta Crystallogr D Biol Crystallogr* **2010**, 66, 133-144.
49. Dodson, E. J.; Winn, M.; Ralph, A. Collaborative computational project, number 4: providing programs for protein crystallography. *Methods Enzymol* **1997**, 277, 620-633.
50. Emsley, P.; Lohkamp, B.; Scott, W. G.; Cowtan, K. Features and development of Coot. *Acta Crystallogr D Biol Crystallogr* **2010**, 66, 486-501.
51. Bricogne, G.; Blanc, E.; Brandl, M.; Flensburg, C.; Keller, P.; Paciorek, W.; Roversi, P.; Sharff, A.; Smart, O. S.; Vonrhein, C.; Womack, T. O. *BUSTER version 2.11.5*. Global Phasing Ltd: Cambridge, United Kingdom, 2011.
52. Chen, V. B.; Arendall, W. B., 3rd; Headd, J. J.; Keedy, D. A.; Immormino, R. M.; Kapral, G. J.; Murray, L. W.; Richardson, J. S.; Richardson, D. C. MolProbity: all-atom structure validation for macromolecular crystallography. *Acta Crystallogr D Biol Crystallogr* **2010**, 66, 12-21.

## Table of Contents graphic



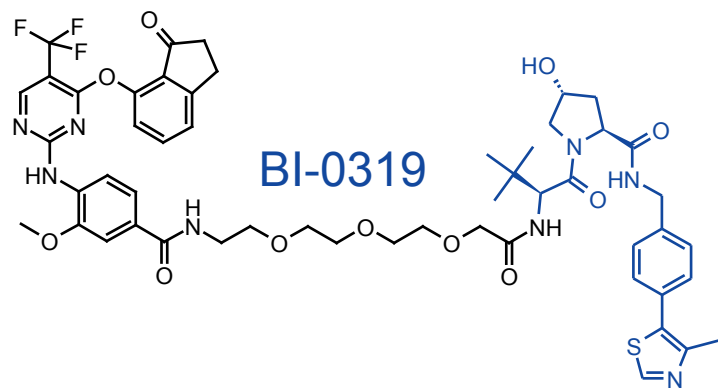
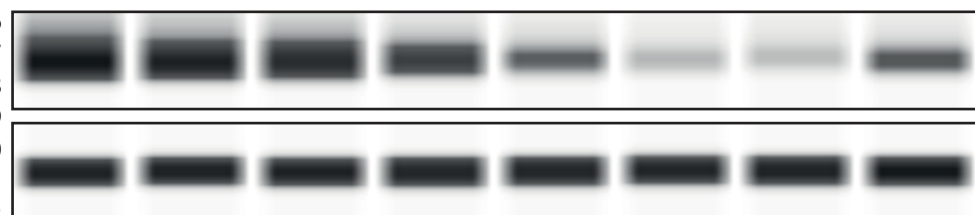
0.01 - 25  $\mu\text{M}$ 

Control



PTK2

GAPDH

0.01 - 25  $\mu\text{M}$ 

PTK2

GAPDH